Learning and Nonlinear Models - Journal of the Brazilian Society on Computational Intelligence (SBIC), Vol. 22, Iss. 1, pp. 61-95, 2024

ADAPTIVE IMMUNE FUZZY QUASI-SLIDING MODE FORMATION TRACKING CONTROL FOR WHEELED MOBILE ROBOTS WITH OBSTACLE AVOIDANCE UNDER INCIDENCE OF UNCERTAINTIES AND DISTURBANCES: AN ARTIFICIAL IMMUNE SYSTEMS INSPIRED APPROACH

Willy John Nakamura Goto
Department of Informatics, Postgraduate Program in Computer Science, State University of Maringá, Paraná, Brazil
willy.john.goto@gmail.com

Douglas Wildgrube Bertol
Department of Electrical Engineering, Systems Automation and Robotics Group, Santa Catarina State University
douglas.bertol@udesc.br

Nardênio Almeida Martins
Department of Automation and Systems, Robotics Research Group, Federal University of Santa Catarina
namartins@uem.br

Resumo – Este artigo apresenta um controle cinemático por modos quasi-deslizantes imunológico adaptativo integrado com um controle dinâmico PD para o rastreamento de trajetória e o controle de formação líder-seguidor por robôs móveis com rodas com acionamento diferencial não-holonômico sob incidência de incertezas e perturbações. Uma abordagem bio-inspirada no mecanismo de regulação imunológica com efeito de reação estabelecido por um novo conjunto de regras fuzzy para ajustar o esforço de controle de forma adaptativa é projetada, uma camada limite fuzzy também é utilizada e uma lei de adaptação para o ajuste on-line de ganho da porção imunológica é introduzida de tal forma a também evitar a deriva paramétrica, lidando com as desvantagens de um controle por modos deslizante de primeira ordem clássico, suprimindo o *chattering* e ainda mantendo a robustez sem conhecimento *a priori* dos limites das perturbações. Também é proposta uma estratégia para desvio de obstáculos por um método reativo e raio de desvio variável. A análise de estabilidade é realizada com base na teoria de Lyapunov. Os resultados de simulação e experimentais demonstram a eficácia do controle proposto.

Palavras-chave – Robôs móveis com rodas, Controle por modos deslizantes, Rastreamento de trajetória e controle de formação líder-seguidor, Sistemas imunológicos artificiais, Incertezas e perturbações, Desvio de obstáculos.

Abstract – This paper presents an adaptive immune fuzzy quasi-sliding mode kinematic control integrated with a PD dynamic control for the trajectory tracking and the leader-follower formation control by nonholonomic differential-drive wheeled mobile robots under incidence of uncertainties and disturbances. An immune regulation mechanism bio-inspired approach with reaction effect established by novel fuzzy rules set to adjust the control effort adaptively is designed, also using a fuzzy boundary layer and introducing an adaptation law for the immune portion gain online adjustment in such a way that they can also avert parameter drift, dealing with the drawbacks of a classic first-order sliding mode control, suppressing chattering and still maintaining the robustness with no *a priori* knowledge of the bounds of the disturbances. An obstacle avoidance strategy with a reactive method and variable avoidance radius is also proposed. The stability analysis is performed based on the Lyapunov theory. Simulation and experimental results demonstrate the proposed control effectiveness.

Keywords – Wheeled mobile robots, Sliding mode control, Leader-follower formation tracking control, Artificial immune systems, Uncertainties and Disturbances, Obstacle avoidance.

1 Introduction

The differential drive wheeled mobile robot (DWMR) is a nonholonomic system and, despite the movement constraints, it is characterized by a simple and low-cost mechanical structure, widely applied in control experiments [1]. In this paper, for the trajectory tracking control problem, is described a robust first-order sliding mode kinematic control (here simply denoted by SMC), depicted by a high-speed switching control law, whose task is to drive the trajectory of states onto a specified region of state-space (known as sliding surface) and keeping it there (a property called by sliding mode) [2]. The extension to the formation control by multiple robots is addressed by adopting the leader-follower separation-bearing strategy for simplicity and the fact that its disadvantage associated with direct error propagation does not significantly affect formations with few DWMRs [3].

Some studies can be cited considering the sliding mode technique in controllers applied to solving these control tasks. For trajectory tracking, a sliding mode kinematic controller using a S-type continuous function instead of signum function and proportional-integral (PI) sliding variable is proposed in [4]. It is proposed, in [5], a sliding mode controller based on a double power reaching law to achieve a higher convergence rate, being the variation in control gains based on an exponential term, and, in replacement of the sign function, the hyperbolic tangent function and another continuous function are applied. Different controllers are proposed in [3] for trajectory tracking and leader-follower formation control, designing adaptive fuzzy systems and neural networks to replace the sliding mode portion of the SMC. The trajectory tracking for a tracked vehicle is addressed in [6], proposing a backstepping kinematic control and, for dynamic control, a SMC considering PI-type sliding surfaces, a continuous approximation replacing the sign function and optimal evaluation of control gains. A backstepping kinematic control is also designed in [7] for a leader-follower formation control of nonholonomic WMRs, and a fractional order SMC with a PI-type sliding surfaces and gains adjusted by a fuzzy system is proposed for dynamic control. In [8], a SMC with a PI sliding variable is also applied for dynamic control, and a self-tuning backstepping controller is employed for kinematic control. In [9], a kinematic controller using the sliding mode technique with a particular sliding variables design is proposed in solving the formation tracking control based on local interactions. In these last two works, a continuous approximation function replaces the sign function, but the control gains are chosen as constants, and a suitable value must still be selected for them.

Considering the importance of leader DWMR safety in the proposed formation control, obstacle avoidance is another pertinent problem required to develop evasive strategies so that the robots can perform their tasks safely. Most works address obstacle avoidance separately from trajectory tracking, generally considering it in the context of autonomous robot navigation problems, determining a reasonable collision-free path between an initial and a final point, such that the robot must reach the target destination. Either way, it is not an easy task because, to ensure the robot's movement, safety, flexibility, and reliability, it is also important to consider the robot's nonholonomic constraints [10, 11]. This paper proposes a strategy based on a reactive approach to avoid collisions of the leader DWMR with static obstacles while tracking the reference trajectory at execution time.

Moreover, an interesting concept is to take inspiration from nature to design controllers capable of achieving their goals without using unnecessary efforts and loss of performance [12].

The artificial immune system (AIS) is an example of a bio-inspired intelligent information processing system, stated in [13] at the beginning of this last decade, as an emerging field of research on control, optimization, pattern recognition, and classification. The adaptive humoral/feedback immunity model was widely applied in PID-type controllers gain adjustment as in [14] for a DWMR control (but without considering effects of the uncertainties and disturbances), and [15–20], for other control systems, to mention a few. However, there is a scarcity of works that combine this type of AIS scheme and the SMC design for DWMRs, being seen applied to different systems and problems in [21–25].

The main contribution of this paper is an adaptive robust control design (denoted by AIFQSMC) for the DWMRs, based on the combination of the sliding mode control technique, artificial immune systems, and fuzzy logic in solving problems of leader-follower formation control, trajectory tracking, obstacle avoidance, robustness to the incidence of uncertainties and disturbances, mitigation of the chattering and also addressing the issue of parametric drift in gain adaptation. To achieve this main contribution, developments judged necessary and no less important are detailed in the following: a simple fuzzy boundary layer approach using saturation function is determined to replace the discontinuous function of the sliding mode portion, significantly avoiding the chattering phenomenon; an AIS scheme is designed for automatically adjusting the gain of the sliding mode portion inspired by an immune response model through a simple fuzzy inference system (FIS) with a new set of fuzzy rules designed according to the immune regulation mechanism, making it feasible to adjust the magnitude of the control effort adaptively and maintaining robustness without requiring any *a priori* knowledge of the bounds of the uncertainties and disturbances or time delays, and attenuating the chattering; an obstacle avoidance strategy based on a reactive method and a variable avoidance radius expansion is proposed to prevent the leader DWMR from colliding with circular-shaped static obstacles distributed along the trajectory while tracking; an adaptation law is established for immune portion gain online adjustment that avoids the parameter drift problem, with its obtaining, within the control law, derived from the the stability analysis of the closed-loop control system through Lyapunov's theory; the effectiveness of the AIFQSMC is evaluated by means of simulations in Matlab/Simulink and experimental simulations using Gazebo/ROS considering kinematic and dynamic models of the PowerBot DWMR, also compared with the SMC and another adaptive controller. Furthermore, alternatively to [26], an auxiliary reference angular velocity is calculated from the inverse kinematics for the leader and followers DWMRs, which allows the formation to maneuver respecting the nonholonomic constraint of non-slipping and considering issues primarily related to the orientation of each DWMR while making a turn.

It is essential to point out that this paper also describes the problem of integrating the AIFQSMC (kinematic control) with a PD control (dynamic control). Similarly to [27], the kinematic control generates velocity control signals to compensate posture tracking errors, providing robustness. They are also set as the references for the dynamic controller, which generate forces and torques that act on the DWMRs to compensate auxiliary tracking velocity errors. As a requirement, the PD control must ensure a stable and fast-tracking of the references despite neglected dynamics to improve the robustness against chattering.

This paper is organized as follows. **Section** 2 presents the DWMR modeling and the description of the trajectory tracking and formation control problems. In the **Section** 3, the kinematic and dynamic control structures (SMC and PD control) are presented. The **Section** 4 is dedicated to performing the control design considering the AIS-inspired approach. The **Section** 5 describes the separation-bearing modeling. Obstacle avoidance by the leader DWMR is treated in **Section** 6. The simulation results are shown and analyzed in **Section** 7, and **Section** 8 concludes this study.

2 Problem Formulation

The leader DWMR is indicated by the subscript i, and the follower DWMRs are identified by subscript j. When the equations refer to the leader only or about modeling the DWMRs in general, without loss of generality, the subscript i will be omitted for readability.

2.1 Kinematic and Dynamic Models of the DWMR

A posture model in space state of DWMRs with uncertainties is described by [3, 28]:

$$\begin{bmatrix} \dot{q} \\ \dot{v} \end{bmatrix} = \begin{bmatrix} J(q)v \\ -\overline{M}^{-1}(q)\left(\overline{H}(q,\dot{q})v + \overline{\tau}_b\right) \end{bmatrix} + \begin{bmatrix} 0 \\ \overline{M}^{-1}(q)\overline{E}(q) \end{bmatrix} \tau \,, \tag{1}$$

where $q = [x\ y\ \theta]^T$ is the posture vector, with the coordinates of the DWMR, (x, y), and orientation, θ; $v = [v_l\ \omega_a]^T$ is the DWMR velocity vector; $\tau = [\tau_r\ \tau_l]^T$ is the torque vector, with the torque in the right wheel, τ_r, and left wheel, τ_l; $\overline{\tau}_b = \Delta\overline{M}(q)\dot{v} + \Delta\overline{H}(q,\dot{q})v + \overline{\tau}_d$ as in [28], representing uncertainties and disturbances on the DWMR's dynamics; $J(q) = [\cos(\theta)\ \sin(\theta)\ 0; -d\sin(\theta)\ d\cos(\theta)\ 1]^T$ is the Jacobian matrix, being d the distance between the center of mass and the intersection point of the symmetry axis of the robot and the wheel axis; $\overline{M}(q) = [m\ 0; 0\ -md^2 + I]$ and $\overline{H}(q,\dot{q}) = [0\ -dm\dot{\theta};\ dm\dot{\theta}\ 0]$ are known smooth nominal functions associated to the inertia and the centripetal and Coriolis matrices, respectively, being m the mass of the DWMR and I the moment of inertia; and $\overline{E}(q) = [r/2\quad r/2;\ r/2b\ \ -r/2b]$ is an input transformation matrix, being r the radius of the actuated wheels and b the distance from the center of an actuated wheel to the DWMR symmetry axis;

The DWMR posture model, Eq. (1), presents the kinematics and dynamics in the first and second lines, respectively, pointing out that the posture model will be used as the basis for the controllers synthesis only.

2.2 Trajectory Tracking

The reference trajectory is generated by a virtual DWMR with the reference posture and velocities known. The aim is to find a smooth velocity control v_c such that $\lim_{t\to\infty}(q_e) = 0$, where q_e is the posture error and v_r is the reference velocity vector. Then the control torque for Eq. (1) is computed such that $v \to v_c$ as $t \to \infty$ [27].

2.3 Leader-Follower Formation Control

The aim of separation-bearing formation control is to find a velocity control input v_{c_j} for the follower DWMR j such that [29]: $\lim_{t\to\infty}(L_{ij_d} - L_{ij}) = 0$ and $\lim_{t\to\infty}(\Psi_{ij_d} - \Psi_{ij}) = 0$, where L_{ij} and Ψ_{ij} are the measured separation distance and bearing angle of the follower j to leader i, with L_{ij_d} and Ψ_{ij_d} being desired separation distance and bearing angle respectively. This same smooth velocity input v_{c_j} must also satisfy $\lim_{t\to\infty}(q_{r_j} - q_j) = 0$. Then torque τ_j for dynamics, Eq. (1), is computed so that $\lim_{t\to\infty}(v_{c_j} - v_j) = 0$ [3].

3 Leader Control Design

3.1 Dynamic Control

The dynamic controller aims to compensate the known torques and forces to ensure fast-tracking of the auxiliary velocity tracking errors, v_e. For the PD control design, as in [3, 27, 28, 30], one considers:

$$\tau = \overline{E}(q)^{-1}\overline{u}\,, \tag{2}$$

applied to the system, Eq. (1). To achieve fast convergence of v_c, the vector $\overline{u} = [\overline{u}_v\ \overline{u}_\omega]^T$ is a control input that will be designed as the PD control, being generated in frequency domain by $C_v(s) = \frac{v(s)}{\overline{u}_v(s)} = (k_{p_v} + k_{d_v}N_v)/(1 + \frac{N_v}{s})$ and $C_\omega(s) = \frac{\omega(s)}{\overline{u}_\omega(s)} = k_{p_\omega} + (k_{d_\omega}N_\omega)/(1 + \frac{N_\omega}{s})$ with $v_e = v_c - v$, the proportional gains k_{p_v} and k_{p_ω}, the derivative gains k_{d_v} and k_{d_ω}, and the derivative filter parameter gains N_v and N_ω being positive and adjusted to achieve stability with good time response performance despite the neglected dynamics, avoiding chattering [28].

This dynamic controller ensures fast convergence of auxiliary velocities tracking errors, as seen in [27,28,30], and it is proved asymptotically stable by Lyapunov's theory considering a constant reference velocity [3]. However, in this paper, the reference velocities are time-varying, which implies the stability of the closed-loop system loses its asymptotic feature. For this reason, the residual error will be handled by the SMC. It is also noteworthy that the kinematic control could handle the entire control problem without the

dynamic control, but since the considered PowerBot DWMR is a closed platform with an internal dynamic control architecture, that is, the control of motor torques is not allowed, the use of PD dynamic controller, as built into the robot, is maintained in the implementations to carry out the simulations.

3.2 Kinematic Control - SMC

The leader kinematic control aim is to set the velocities required so that the DWMR can track the virtual DWMR. Being $q_r = [x_r\ y_r\ \theta_r]^T$ and $v_r = [v_{lr}\ \omega_{ar}]^T$ as the reference posture and velocity vectors respectively, the virtual DWMR kinematics is modeled as:

$$\dot{q}_r = \begin{bmatrix} \dot{x}_r \\ \dot{y}_r \\ \dot{\theta}_r \end{bmatrix} = \begin{bmatrix} \cos(\theta_r) & 0 \\ \sin(\theta_r) & 0 \\ 0 & 1 \end{bmatrix} \begin{bmatrix} v_{l_r} \\ \omega_{a_r} \end{bmatrix} . \tag{3}$$

Based on the reference and DWMR postures, the posture tracking errors are obtained in the inertial frame to the DWMR frame, and then the leader DWMR i posture error is obtained as:

$$q_e = \begin{bmatrix} x_e \\ y_e \\ \theta_e \end{bmatrix} = \begin{bmatrix} \cos(\theta) & \sin(\theta) & 0 \\ -\sin(\theta) & \cos(\theta) & 0 \\ 0 & 0 & 1 \end{bmatrix} \begin{bmatrix} x_r - x \\ y_r - y \\ \theta_r - \theta \end{bmatrix} . \tag{4}$$

Due to nonholonomy and $d \neq 0$, the leader orientation will not be equal to the virtual DWMR orientation while making a turn, and the reference orientation cannot be as $\theta_r = \theta$ [26]. So, from the inverse kinematics, auxiliary reference velocities can be given as:

$$\begin{bmatrix} v_{lr}^* \\ \omega_{ar}^* \end{bmatrix} = \begin{bmatrix} v_{lr}\cos(\theta_r^* - \theta_r) \\ -\dfrac{1}{d} v_{lr}\sin(\theta_r^* - \theta_r) \end{bmatrix} . \tag{5}$$

Since the "perfect velocity tracking" ($v = v_c$) does not hold into practice, some bounded auxiliary velocity tracking errors v_e are generated, which can be transcribed as effects of the uncertainties and disturbances $\tilde{d}_0$ for the kinematics [27]. Thus, based on a generic modeling of nonlinear systems, the error dynamics of the closed-loop system is obtained as follows:

$$\begin{aligned} \dot{q}_e &= A_0(q_e,t) + B_0(q_e,t)v_c(t) + d_b(q,t) \\ \begin{bmatrix} \dot{x}_e \\ \dot{y}_e \\ \dot{\theta}_e^* \end{bmatrix} &= \begin{bmatrix} v_{lr}\cos(\theta_e) \\ v_{lr}\sin(\theta_e) \\ \omega_{ar}^* \end{bmatrix} + \begin{bmatrix} -1 & y_e \\ 0 & -(d + x_e) \\ 0 & -1 \end{bmatrix} \begin{bmatrix} v_{lc} + \tilde{d}_{0_v} \\ \omega_{ac} + \tilde{d}_{0_\omega} \end{bmatrix} , \end{aligned} \tag{6}$$

where $A_0(q_e,t)$ and $B_0(q_e,t)$ refer to the vector and matrix of nominal parameters, respectively, and $v_c(t)$ is the vector of control inputs. The effects of the disturbances $\tilde{d}_{0_v}$ and $\tilde{d}_{0_\omega}$ are assumed to be bounded by positive constants as $|\tilde{d}_{0_v}| \leq \tilde{d}_{0_{M_v}}$ and $|\tilde{d}_{0_\omega}| \leq \tilde{d}_{0_{M_\omega}}$, or norm-bounded by $\|\tilde{d}_0\| \leq \tilde{d}_{0_M}$.

Having the posture error dynamics established, with $\theta_{\mathrm{e}}^* = \theta_{\mathrm{r}}^* - \theta$, the sliding surfaces are chosen as:

$$\sigma = \begin{bmatrix} \sigma_v \\ \sigma_\omega \end{bmatrix} = \begin{bmatrix} \lambda_1 x_e \\ \lambda_2 y_e + \lambda_3 \theta_e^* \end{bmatrix} , \tag{7}$$

where λ_1, λ_2 and λ_3 are positive constants.

Using Eqs. (6) and (7), one has:

$$\begin{aligned} \dot{\sigma}(q_e,t) &= \frac{\partial \sigma(q_e,t)}{\partial q_e}\dot{q_e} + \frac{\partial \sigma(q_e,t)}{\partial t} \\ &= A_{0_\sigma} + B_{0_\sigma} v_c + d_\sigma + \frac{\partial \sigma}{\partial t} \end{aligned} , \tag{8}$$

where $A_{0_\sigma} = \frac{\partial \sigma}{\partial q_e} A_0$, $B_{0_\sigma} = \frac{\partial \sigma}{\partial q_e} B_0$ and $d_\sigma = \frac{\partial \sigma}{\partial q_e} d_b = \frac{\partial \sigma}{\partial q_e} B_0 \tilde{d}_0$ represents the effects of the uncertainties and disturbances on the system.

However, to solve a nonsingularity problem of B_{0_σ}, as described in more detail in [3,27], new sliding surfaces ($\sigma^* = [\sigma_v^*\ \sigma_\omega^*]^T$) are required to be established as:

$$\begin{aligned} \sigma^* &= B_{0_\sigma}^T \sigma; \\ \sigma_v^* &= -\lambda_1^2 x_e \\ \sigma_\omega^* &= \lambda_1^2 y_e x_e - \left[\lambda_2(d + x_e) + \lambda_3\right](\lambda_2 y_e + \lambda_3 \theta_e^*) \end{aligned} \tag{9}$$

It is pointed out that the SMC aims to obtain a sliding motion restricted to $\sigma(q_e,t) \to 0$, $\dot{\sigma}(q_e,t) \to 0$, $\sigma^*(q_e,t) \to 0$ and $\dot{\sigma}^*(q_e,t) \to 0$.

For the stability analysis, the Lyapunov candidate function is selected as:

$$V = \frac{1}{2}\sigma^T\sigma\,, \tag{10}$$

which is positive definite ($V > 0$).

The control law is derived as [3, 27]:

$$v_{\rm c} = \underbrace{-B_{0_\sigma}^{-1}A_{0_\sigma}}_{\text{equivalent control}} - \underbrace{G\,\text{sign}(\sigma^*)}_{\text{sliding mode}} \underbrace{-P\sigma^*}_{\text{reaching mode}} \tag{11}$$

where $\text{sign}(\sigma_n^*) = |\sigma_n^*|/\sigma_n^*$ and

$$A_{0_\sigma} = \begin{bmatrix} \lambda_1 v_{lr}\cos(\theta_e) \\ \lambda_2 v_{lr}\sin(\theta_e) + \lambda_3\omega_{ar}^* \end{bmatrix}\,, \tag{12}$$

$$B_{0_\sigma}^{-1} = \begin{bmatrix} -\dfrac{1}{\lambda_1} & -\dfrac{y_e}{\lambda_2(d+x_e)+\lambda_3} \\ 0 & -\dfrac{1}{\lambda_2(d+x_e)+\lambda_3} \end{bmatrix}\,, \tag{13}$$

where $\lambda_2 = \lambda_3\,\alpha_\sigma$, with $0 \leq \alpha_\sigma \leq 1/(||d+x_e||+1)$, need to be satisfied for the matrix $B_{0_\sigma}^{-1}$ to always be nonsingular.

By differentiating Eq. (10), considering Eq. (8) and the control law Eq. (11), one obtains:

$$\begin{aligned} \dot{V} = \sigma^T\dot{\sigma} &= -{\sigma^*}^T G\text{sign}(\sigma^*) - {\sigma^*}^T P\sigma^* + {\sigma^*}^T\tilde{d}_0 \\ &\leq -{\sigma^*}^T P\sigma^* - \left(\lambda_{\min}\{G\} - \tilde{d}_{0_M}\right)\|\sigma^*\|. \end{aligned} \tag{14}$$

Since ${\sigma^*}^T P\sigma^* \geq 0$, the condition $\dot{V} \leq 0$ is satisfied when $\lambda_{\min}\{G\} > \tilde{d}_{0_M}$, being $\lambda_{\min}\{G\}$ the minimum singular value of G and $\tilde{d}_{0_M}$, the maximum effects of the disturbances. Hence, it can be seen that if the uncertainties are better estimated, the results will be better [27].

4 AIS Inspired Control Design

4.1 Humoral Immune Response Mechanism

The main role of the biological immune system (BIS) is to identify and eliminate foreign bodies called antigens, being the collective and coordinated response of the cells responsible for it known as immune response. There are two types of immunity [31]: As the first line of defense, the innate immune system reacts to all pathogens; the adaptive immune system is directed against specific antigens whose immune responses are classified into cell-mediated immunity and humoral immunity. This paper considers the last one to design the proposed AIS control structure. The cells responsible for adaptive humoral immunity are white blood cells (leucocytes) called lymphocytes, being the main ones B cells and T cells. The B cells are associated with the production of antibodies (Ab) that attack a specific antigen (Ag). Meanwhile, T cells need antigen-presenting cells (APC) to be activated. The immunity regulation is mainly performed by T helper cells (T_h), which secrete interleukin IL^+ that stimulate B cells to produce antibodies, and suppressor T cells (T_s), which, by producing interleukin IL^-, restrict the action of T_h and B cells to prevent excessive immune responses, leading to the response stabilization. The simplified humoral immunity behavior can be illustrated according to Fig. 1.

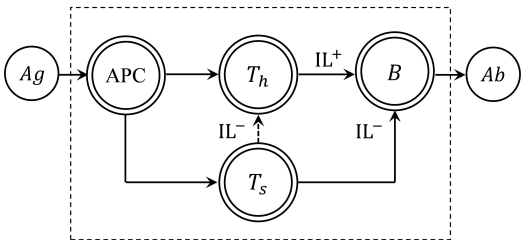

Figure 1: Illustrative diagram of humoral immunity.

Generally, projects of AIS based on this type of mechanism focus on the restrictive action on B cells. So, similarly to [16], the corresponding parts of humoral-type AIS structure can be obtained as follows:

$$T_h = k_h(\varepsilon); \tag{15}$$
$$T_s = k_s(\varepsilon) f(\varepsilon, \Delta\varepsilon); \tag{16}$$

$$\begin{aligned} S_B &= T_h - T_s \\ &= k_h(\varepsilon) - k_s(\varepsilon) f(\varepsilon, \Delta\varepsilon) \ , \\ &= k_h(\varepsilon)[1 - \eta f(\varepsilon, \Delta\varepsilon)] \end{aligned} \tag{17}$$

where $\eta = k_s(\varepsilon)/k_h(\varepsilon)$ is a proportionality factor describing the interaction between T_h and T_s cells, ε is the amount of the antigens and $\Delta\varepsilon$ its variation, T_h and T_s denotes the action of T_h and T_s cells respectively, S_B is the total stimulation received by B cells, k_h is the enhancing factor, k_s is the supressing factor and $f(\cdot)$ is a nonlinear function that represents the immune reaction effect. Table 1 outlines the control system course compared to the immune regulation process [20, 32].

Table 1: Immune reactions and adaptive control comparative.

Immune reaction	Adaptive control
Facing an invasion of foreign materials, when the first line of defense (innate immunity) fails, the amount of antigens is higher, and the production of antibodies is expected to increase rapidly, so the inhibitory action of T_s cells must be contained to promote greater stimulation.	If robustness fails (control action is unsatisfactory or system is unstable or disturbed), an estimate of the limits of the disturbances is presented to generate an "antibody" equivalent to modifying the control system.
With antigen reduction, the amount of antibodies is not expected to increase continuously. In other words, the containment on T_s cells should decrease.	Based on some performance measure, the parameters of the control system can be adaptively adjusted.
When most of the antigens have been removed, the suppression stimulus of T_s cells is expected to rapidly increase to restrict B cells and antibody production, stabilizing the immune reactions.	When the observed errors indicate a reduction, the control system output is computed to minimize control efforts and achieve control system stability.

4.2 Adaptive Immune Fuzzy Quasi-Sliding Mode Control (AIFQSMC)

Given the concepts described, this humoral immune mechanism can be introduced for adaptive regulation of the sliding mode portion gain to minimize the control efforts and compensate for disturbances.

For this, it was established that the amount of the antigens is the sliding surface σ^*, as in [21–25], and total stimulation received by B cells for antibody generation corresponds to the sliding mode portion gain ($G_{AIS} = k_h - k_s f(\sigma^*, \dot{\sigma}^*)$) as shown in Fig. 2.

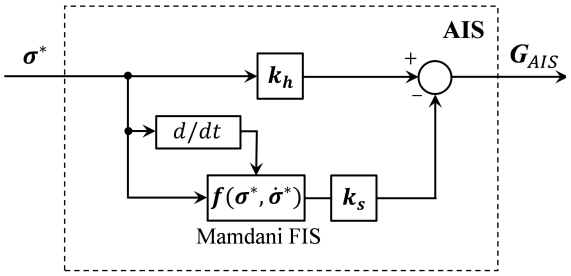

Figure 2: Proposed AIS control structure.

It can be seen that the nonlinear function $f(\cdot)$ plays an important role related to the regulation of the stimulus received by B cells since the reaction can be defined by the activation or containment of the effect of T_s cells. In some works, $f(\cdot)$ is described by an exponential function based on antigen consistency as in [17, 22, 23, 25]. A fuzzy system is alternatively used as in [15–21, 24], which usually considers the total stimulation received by B cells and its variation with an immune response delay. In this paper, it is proposed the reaction effect based on the antigen amount and its variation, without the need to apply a time delay, as illustrated in Fig. 2, according to the principles described in Section 4.1.

So, taking advantage of the universal approximation property, simplicity, and intuitive linguistic interpretation, a Mamdani FIS is designed to compute the nonlinear function $f(\sigma^*, \dot{\sigma}^*)$. With N input variables, M output variables, and triangular membership functions, by adopting the singleton fuzzification, the product inference engine, the center average defuzzification method, and a set of K "if...then..." fuzzy rules, the mth crisp output of the FIS, y_m, can be obtained by [33]:

$$y_m = \frac{\sum_{k=1}^{K} c_m^{(k)} s_k}{\sum_{k=1}^{K} s_k} = C^T \xi(x)\,, \tag{18}$$

where $c_m^{(k)}$ is the center value of the *m*th output membership function (MF) in the *k*th fuzzy rule, $s_k = \prod_{n=1}^{N} \mu_n^{(k)}(x_n)$ is the product of MFs' mappings for all input variables in the *k*th fuzzy rule, being μ_n the membership function of the input x_n ($n = 1, \ldots, N$) and $\xi(x) = \left(\xi^{(1)}(x), \ldots, \xi^{(K)}(x)\right)^T$ is a regressive vector with $\xi^{(k)}(x) = s_k / \sum_{k=1}^{K} s_k$.

In this paper, the non-linear function $f(\cdot)$ is the output of the fuzzy controller, whereas σ^* and $\dot{\sigma}^*$ are the inputs. The fuzzy rules were designed according to the immune regulation mechanism principles summarized in Table 1 and can be inferred as shown in Table 2, where NB is Negative Big, NM is Negative Middle, NS is Negative Small, ZO is Zero, PS is Positive Small, PM is Positive Middle and PB is Positive Big. Since σ^* can assume positive and negative values, it can be interpreted, in summary, that there is an antigen amount in distinct semi-cycles: positive and negative. This means that a positive value for σ^* and a positive variation ($\dot{\sigma}^* > 0$), or a negative value for σ^* and $\dot{\sigma}^* < 0$ denote an increase in antigen amount, whereas $\sigma^* > 0$ and $\dot{\sigma}^* < 0$, or $\sigma^* < 0$ and $\dot{\sigma}^* > 0$ indicates a reduction in antigens amount. If σ^* and $\dot{\sigma}^*$ are close to zero, respectively, it indicates that there is no significant amount and no significant variation has occurred.

Moreover, f is bounded, and $f \leq 0$ represents a containment of the suppression effect, that is, the stimulus is enhanced, whereas $f > 0$ denotes a promotion of the inhibitory effect to smooth the control effort.

Table 2: Fuzzy rules for nonlinear function $f(\cdot)$

			$\dot{\sigma}^*$		
σ^*	NB	NS	ZO	PS	PB
NB	NB	NM	NM	NS	NS
NS	NM	NS	ZO	PS	ZO
ZO	ZO	PS	PM	PS	ZO
PS	ZO	PS	ZO	NS	NM
PB	NS	NS	NM	NM	NB

Terms k_h and k_s can be positive constants, as in [21] and [24], but can also be variables based on antigens amount (e.g., linear/nonlinear function or adaptive parameter), as in [22], [23], [25]. In this paper, gains k_s are considered positive constants, and avoiding the choice by trial and error, an adaptation law is proposed to estimate online the gains k_h.

In the proposed controller, $\mathrm{sign}(\sigma^*)$ was replaced by $\mathrm{sat}(\sigma^*)$, whose *n*th element is defined as:

$$\mathrm{sat}(\sigma_n^*) = \begin{cases} \mathrm{sign}(\sigma_n^*) & \text{if } |\sigma_n^*| > \beta_n \\ \dfrac{\sigma_n^*}{\beta_n} & \text{if } |\sigma_n^*| \leq \beta_n \end{cases}, \tag{19}$$

in which $\beta_n > 0$ defines the *n*th value of the boundary layer thickness. This alternative has a price that the attractiveness is no longer ensured to zero but to a closed region defined by the boundary layer (BL), in which the discontinuous control signal is smoothed [34, 35].

The AIFQSMC control law can be established as follows:

$$v_c = -B_{0_\sigma}^{-1} A_{0_\sigma} - \hat{G}_{AIS}\mathrm{sat}(\sigma^*) - P\sigma^* \tag{20}$$

where $\hat{G}_{AIS} = \hat{k}_h - k_s f(\sigma^*, \dot{\sigma}^*)$ is described by diagonal matrices. Alternatively, $\hat{G}_{AIS} = \hat{k}_h[1 - \hat{\eta} f(\sigma^*, \dot{\sigma}^*)]$, with $\hat{\eta} = k_s / \hat{k}_h$.

A possible unboundedness of gains estimates when the PE condition fails to hold (signals are not persistently exciting) is known as parameter drift, which can be caused by non-idealities on the system, being characterized as one of the significant problems associated with parametric uncertainties [36, 37]. To deal with the mentioned parameter drift, based on the approach of [38], the proposed adaptation law for *n*th estimated value $\hat{k}_h$ can be as:

For $|\sigma_n^*| > \beta_n$,

$$\dot{\hat{k}}_{h_n} = \begin{cases} \Gamma_{h_n} |\sigma_n^*| \mathrm{sign}(|\sigma_n^*| - \epsilon_n) & \text{if } \hat{k}_{h_n} > \overline{k}_{h_n} \\ \overline{k}_{h_n} & \text{if } \hat{k}_{h_n} \leq \overline{k}_{h_n} \end{cases} \tag{21}$$

and, for $|\sigma_n^*| \leq \beta_n$,

$$\dot{\hat{k}}_{h_n} = \begin{cases} \Gamma_{h_n} (|\sigma_n^*|^2 / \beta_n) \mathrm{sign}(|\sigma_n^*| - \epsilon_n) & \text{if } \hat{k}_{h_n} > \overline{k}_{h_n} \\ \overline{k}_{h_n} & \text{if } \hat{k}_{h_n} \leq \overline{k}_{h_n} \end{cases} \tag{22}$$

with $\hat{k}_{h_n}(t = 0) > 0$, $\epsilon_n > 0$, $\beta_n > 0$, and a small enough positive parameter $\overline{k}_{h_n}$, which is introduced to obtain only positive values for $\hat{k}_{h_n}$. $\Gamma_{h_n} > 0$ is a term that denotes the adaptation gain, which may be related to the adjustment rate of the adaptive

parameter, with its increase usually influencing the reduction of convergence time, but paying attention that values that are too high can induce unnecessary overcharging. It is worth remembering that, according to the approach used in the adaptation law, there is not only an increase factor but also a reduction factor for the adaptive gain, which is inserted within the AIS as one of the parts that make up the gain $\hat{G}_{AIS}$.

The adaptation laws, by Eqs. (21) and (22), allow not only the gain $\hat{k}_{h_n}$ increasing but also declining due the additional term $\text{sign}(|\sigma_n^*| - \epsilon_n)$. The gain $\hat{k}_{h_n}$ increases while $|\sigma_n^*| > \epsilon_n$ and decreases while $|\sigma_n^*| < \epsilon_n$. So, since the change in the value of $\hat{k}_{h_n}$ is determined by $\dot{\hat{k}}_{h_n}$, it tends to be smaller as $|\sigma_n^*|$ approaches ϵ_n and the adaptation process stops when the sliding variable reaches it ($|\sigma_n^*| = \epsilon_n$) [38, 39]. In other words, the gain will be kept at the smallest level, allowing a determined accuracy of σ^*-stabilization at an eminent cost that this approach ensures a real sliding mode only. It is assumed succinctly that the sliding variable tends to converge into a region delimited by a margin around zero [40, 41]. When considering the individual adaptive gain ($\hat{k}_h$), the main focus is not to use it precisely to estimate the bounds of the uncertainties and disturbances [42]. Since the gain is inserted in an immune-inspired approach in this work, the estimation of the control effort magnitude for compensatory effect is handled by the AIS gain as a whole, i.e., $\hat{G}_{AIS}$.

It may also be convenient to tune the boundary layer thickness. In [43], a chattering measure is introduced as the absolute value of the derivative of the control signal, $|\dot{v}_c|$, considered as a FIS input variable with the sliding surface to compute the boundary layer alteration. With an exponential relation to regulate the control effort of the reaching law, this concept also inspired the conception of the AIS-based SMC in [25]. Although this approach suggests more dynamic adaptability by taking into account the chattering level, and since the immune control already relies on a regulation process from the function $f(\cdot)$ by a FIS, to provide an online adjustment of the boundary layer thickness, also avoiding time delays, it was opted to implement a Mamdani FIS considering as input only the absolute value of sliding surfaces $|\sigma_n^*|$ with the boundary layer thickness β_n as the output variables, similarly to [44].

For the FIS design, the following principles can be brought up [25, 44]: When the sliding surface is far from the sliding manifold $\sigma_n^* = 0$, a thin BL is required for a faster convergence; When it is closer to the sliding manifold $\sigma_n^* = 0$, a larger boundary layer is desired to mitigate chattering. According to these concepts, the fuzzy rules are designed as presented in Table 3, where VB means Very Big, B is Big, M is Middle, S is Small, and VS is Very Small [44].

Table 3: Fuzzy rules (adaptive variable boundary layer)

Rule	Antecedent	Consequent
R1	IF $\|\sigma_n^*\|$ is VB	THEN β_n is VS
R2	IF $\|\sigma_n^*\|$ is B	THEN β_n is S
R3	IF $\|\sigma_n^*\|$ is M	THEN β_n is M
R6	IF $\|\sigma_n^*\|$ is S	THEN β_n is B
R5	IF $\|\sigma_n^*\|$ is VS	THEN β_n is VB

The fuzzy output is obtained similarly to the Eq. (18). Just note that, while in the FIS designed for AIS function $f(\cdot)$, each output is related to two inputs (i.e., f_v to σ_v^* and $\dot{\sigma}_v^*$ as well as f_ω is to σ_ω^* and $\dot{\sigma}_\omega^*$), this fuzzy system used to compute the boundary layer values have each output associated to only one input (i.e., β_v to $|\sigma_v^*|$ and β_ω to $|\sigma_\omega^*|$). Moreover, since it is computed by a Mamdani FIS, β_n is bounded such as $0 \leq \beta_{n_m} \leq \beta_n \leq \beta_{n_M}$.

Another point is that the parameter ϵ, in Eqs. (21) and (22),

is also called a boundary layer because of gain adaptation behavior as a function of the relation between the sliding surface and a margin value determined by ϵ, but pointing out that it can be different from the boundary layer used in the continuous function replacing the discontinuous switching function [45]. Both are chosen to find a trade-off between accuracy and chattering reduction, but keep in mind that, in this work, the selection of ϵ is also related to parameter drift avoidance. The gain adaptation according to σ^* about ϵ can be described as follows. If ϵ is very small, σ^* may fluctuate so that $\|\sigma^*\| > \epsilon$ and then the gain may increase too much, inducing chattering or even instability. If ϵ is too large, the gain tends to reduce quickly, preventing it from continuing to grow for a long time, but the accuracy may be not good as possible since the system sensitivity is reduced, that is, stimulus activation for compensation of the disturbances only happens if the sliding surface becomes greater than a high value of margin, and gain takes longer to increase and act to reduce errors [38, 46, 47]. In [38, 47], a ϵ-tuning procedure is proposed. Differently, in this work, as the saturation function approach in a quasi-sliding mode control is being used, it aims that the σ^* is attracted and remains inside the boundary layer. In this way, it can be assumed the conception that when the sliding surface gets out of the boundary layer, the stimulus action should be enhanced, making the gain $\hat{k}_h$ increase. An indicator of system stability is when σ^* is within the boundary layer, where the gain can stop increasing and decrease. Then, it was decided to adopt a constant value for the parameter ϵ as a margin that will define the increase or reduction of $\hat{k}_h$. Accordingly, for each *n*th value, it is advisable to adopt $\epsilon_n \geq \beta_n$, looking for a trade-off between performance, chattering, and parameter drift avoidance. So, seeing that a fuzzy boundary layer was applied, an apt value would be $\epsilon_n = \beta_{n_M}$. The AIFQSMC scheme can be illustrated by Fig. 3 for better visualization. Furthermore, in the sequel, similarly as in [38], for discussion and stability analysis proof, and without loss of generality but for the sake of clarity, it is assumed that $\hat{k}_{h_n}(t) > \overline{k}_{h_n}$ for all $t > 0$. As soon, it is seen that a lower bound for $\hat{k}_h$ is evident since, by Eqs. (21) and (22), if its *n*th value $\hat{k}_{h_n} \leq \overline{k}_{h_n}$, then $\dot{\hat{k}}_{h_n}$ is delimited by a minimum value $\overline{k}_{h_n}$.

For the stability analysis, the Lyapunov candidate function is chosen as:

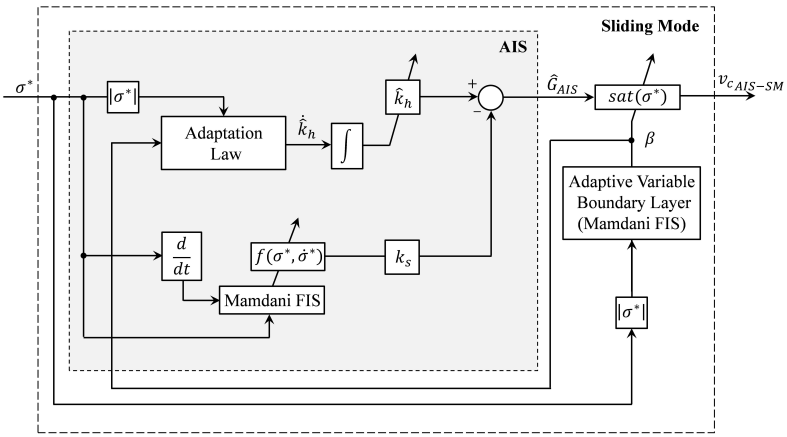

Figure 3: Sliding mode portion of the proposed AIFQSMC control structure.

$$V = \frac{1}{2}\sigma^T\sigma + \frac{1}{2}\sum_{n=1}^{N}\tilde{k}_{h_n}^T\Gamma_{h_n}^{-1}\tilde{k}_{h_n} \ . \tag{23}$$

Since $\Gamma_{h_n} > 0$ for all n, one checks that V is positive definite ($V > 0$). $\tilde{k}_{h_n}$ define the *n*th gain estimation error, given as:

$$\tilde{k}_{h_n}^T = \tilde{k}_{h_n} = \hat{k}_{h_n} - k_{h_n} \ . \tag{24}$$

Differentiating V (Eq. (23)), considering Eq. (8) and $\frac{\partial\sigma}{\partial t} = 0$, one has:

$$\begin{aligned}\dot{V} &= \sigma^T\dot{\sigma} + \sum_{n=1}^{N}\tilde{k}_{h_n}\Gamma_{h_n}^{-1}\dot{\tilde{k}}_{h_n} \\ &= {\sigma^*}^T B_{0_\sigma}^{-1}A_{0_\sigma} + {\sigma^*}^T(v_c + \tilde{d}_0) + \sum_{n=1}^{N}\tilde{k}_{h_n}\Gamma_{h_n}^{-1}\dot{\hat{k}}_{h_n} \ .\end{aligned} \tag{25}$$

Replacing the control law, Eq. (20), one has:

$$\dot{V} = -{\sigma^*}^T(\hat{k}_h - k_s f)\mathrm{sat}(\sigma^*) - {\sigma^*}^T P\sigma^* + {\sigma^*}^T\tilde{d}_0 + \sum_{n=1}^{N}\tilde{k}_{h_n}\Gamma_{h_n}^{-1}\dot{\hat{k}}_{h_n} \ . \tag{26}$$

In the case $|\sigma_n^*| > \beta_n$, one has $\mathrm{sat}(\sigma_n^*) = \mathrm{sign}(\sigma_n^*)$. Selecting the adaptation law from Eq. (21), by replacing it in Eq. (26), one yields to:

$$\dot{V} = -{\sigma^*}^T(\hat{k}_h - k_s f)\mathrm{sign}(\sigma^*) - {\sigma^*}^T P\sigma^* + {\sigma^*}^T\tilde{d}_0 + \sum_{n=1}^{N}\tilde{k}_{h_n}|\sigma_n^*|\mathrm{sign}(|\sigma_n^*| - \epsilon_n) \ . \tag{27}$$

With ${\sigma^*}^T\tilde{d}_0 = \sum_{n=1}^{N}\tilde{d}_{0_n}\sigma_n^* \leq \sum_{n=1}^{N}\tilde{d}_{0_{M_n}}|\sigma_n^*|$ and ${\sigma^*}^T(\hat{k}_h - k_s f)\mathrm{sign}(\sigma^*) = \sum_{n=1}^{N}(\hat{k}_{h_n} - k_{s_n}f_n)|\sigma_n^*|$, one results in:

$$\dot{V} \leq -\sum_{n=1}^{N}\left[(\hat{k}_{h_n} - k_{s_n}f_n)|\sigma_n^*| - \tilde{d}_{0_{M_n}}|\sigma_n^*|\right] - {\sigma^*}^T P\sigma^* + \sum_{n=1}^{N}\tilde{k}_{h_n}|\sigma_n^*|\mathrm{sign}(|\sigma_n^*| - \epsilon_n) \ . \tag{28}$$

By considering the case in which $|\sigma_n^*| > \epsilon_n$, one has that $\mathrm{sign}(|\sigma_n^*| - \epsilon_n) = 1$, then obtaining:

$$\dot{V} \leq -\sum_{n=1}^{N}\left[(\hat{k}_{h_n} - k_{s_n}f_n)|\sigma_n^*| - \tilde{d}_{0_{M_n}}|\sigma_n^*|\right] - {\sigma^*}^T P\sigma^* + \sum_{n=1}^{N}\tilde{k}_{h_n}|\sigma_n^*| \ . \tag{29}$$

One checks that ${\sigma^*}^T P\sigma^* \geq 0$. But, for $\dot{V} \leq 0$, the following conditions must be satisfied:

$$\sum_{n=1}^{N}(\hat{k}_{h_n} - k_{s_n}f_n) \geq \sum_{n=1}^{N}\tilde{d}_{0_{M_n}} \ \text{ and } \ \sum_{n=1}^{N}\tilde{k}_{h_n}|\sigma_n^*| \leq 0 \ . \tag{30}$$

For this condition to be met, seeing estimation error,

$$\sum_{n=1}^{N} \tilde{k}_{h_n}|\sigma_n^*| = \sum_{n=1}^{N}(\hat{k}_{h_n} - k_{h_n})|\sigma_n^*| \leq 0 \ . \tag{31}$$

Thereby, if $\hat{k}_{h_n} \leq k_{h_n}$ and $\hat{k}_{h_n} - k_{s_n} f_n \geq \tilde{d}_{0_{M_n}}$ for all n, then $\dot{V} \leq 0$.

This suggests that there should be an ideal value represented by the scalar k_{h_n} such that $k_{h_n} \geq \hat{k}_{h_n}$. To make it clearer, it is also possible to rewrite the $\dot{V}$, Eq. (29), taking into account the gain estimation error and calling $p_\sigma = {\sigma^*}^T P \sigma^*$, one yields to:

$$\begin{aligned} \dot{V} &\leq -\sum_{n=1}^{N}\left[(\hat{k}_{h_n} - k_{s_n} f_n)|\sigma_n^*| - \tilde{d}_{0_{M_n}}|\sigma_n^*|\right] - p_\sigma + \sum_{n=1}^{N}(\hat{k}_{h_n} - k_{h_n})|\sigma_n^*| \\ &\leq -p_\sigma - \sum_{n=1}^{N}\left[(k_{h_n} - k_{s_n} f_n)|\sigma_n^*| - \tilde{d}_{0_{M_n}}|\sigma_n^*|\right] \ . \end{aligned} \tag{32}$$

Thus, being $p_\sigma \geq 0$, if $k_{h_n} - k_{s_n} f_n \geq \tilde{d}_{0_{M_n}} > 0$ for all n, then $\dot{V} \leq 0$ is satisfied.

When considering the case where $|\sigma_n^*| < \epsilon_n$, one has that $\text{sign}(|\sigma_n^*| - \epsilon_n) = -1$, Eq. (28), becomes:

$$\dot{V} \leq -\sum_{n=1}^{N}\left[(\hat{k}_{h_n} - k_{s_n} f_n)|\sigma_n^*| - \tilde{d}_{0_{M_n}}|\sigma_n^*|\right] - {\sigma^*}^T P \sigma^* - \sum_{n=1}^{N}\tilde{k}_{h_n}|\sigma_n^*| \ . \tag{33}$$

To obtain $\dot{V} \leq 0$, since ${\sigma^*}^T P \sigma^* \geq 0$, the following conditions must be satisfied:

$$\sum_{n=1}^{N}(\hat{k}_{h_n} - k_{s_n} f_n) \geq \sum_{n=1}^{N}\tilde{d}_{0_{M_n}} \tag{34}$$

and, considering the gain estimation error as Eq. (24),

$$\sum_{n=1}^{N} \tilde{k}_{h_n}|\sigma_n^*| = \sum_{n=1}^{N}(\hat{k}_{h_n} - k_{h_n})|\sigma_n^*| \geq 0 \ . \tag{35}$$

Thus, if $\hat{k}_{h_n} \geq k_{h_n}$ and $\hat{k}_{h_n} - k_{s_n} f_n \geq \tilde{d}_{0_{M_n}}$ for all n, then $\dot{V} \leq 0$. Similarly, when considering the case where $|\sigma_n^*| = \epsilon_n$, one has that $\text{sign}(|\sigma_n^*| - \epsilon_n) = 0$, thus $\dot{V}$, Eq. (28), becomes:

$$\dot{V} \leq -p_\sigma - \sum_{n=1}^{N}\left[(\hat{k}_{h_n} - k_{s_n} f_n)|\sigma_n^*| - \tilde{d}_{0_{M_n}}|\sigma_n^*|\right] \ . \tag{36}$$

Since $p_\sigma \geq 0$, for $\dot{V} \leq 0$, the condition $\hat{k}_{h_n} - k_{s_n} f_n \geq \tilde{d}_{0_{M_n}}$ has to be met for all n.

Now, by analysing the case in which $|\sigma_n^*| \leq \beta_n$, one has that $\text{sat}(\sigma_n^*) = \sigma_n^*/\beta_n$. Thus, with similar procedures previously performed, replacing the adaptation law, Eq. (22), the Eq. (26) becomes:

$$\dot{V} = -{\sigma^*}^T(\hat{k}_h - \hat{k}_s f)\frac{\sigma^*}{\beta} - {\sigma^*}^T P \sigma^* + {\sigma^*}^T \tilde{d}_0 + \sum_{n=1}^{N}\tilde{k}_{h_n}\frac{|\sigma_n^*|^2}{\beta_n}\text{sign}(|\sigma_n^*| - \epsilon_n) \ . \tag{37}$$

Similarly as done to obtain Eq. (28), the Eq. (37) can be rewritten as:

$$\dot{V} \leq -\sum_{n=1}^{N}\left[\left((\hat{k}_{h_n} - k_{s_n} f_n)\frac{|\sigma_n^*|}{\beta_n} - \tilde{d}_{0_{M_n}}\right)|\sigma_n^*|\right] - p_\sigma + \sum_{n=1}^{N}\tilde{k}_{h_n}\frac{|\sigma_n^*|^2}{\beta_n}\text{sign}(|\sigma_n^*| - \epsilon_n) \ . \tag{38}$$

Since $\epsilon_n = \beta_{n_M}$ was adopted, the case where $|\sigma_n^*| > \epsilon_n$ will not be treated.

When considering the case where $|\sigma_n^*| < \epsilon_n$, one has that $\text{sign}(|\sigma_n^* - \epsilon_n) = -1$, thus Eq. (38) becomes:

$$\dot{V} \leq -\sum_{n=1}^{N}\left[\left((\hat{k}_{h_n} - k_{s_n} f_n)\frac{|\sigma_n^*|}{\beta_n} - \tilde{d}_{0_{M_n}}\right)|\sigma_n^*|\right] - p_\sigma - \sum_{n=1}^{N}\tilde{k}_{h_n}\frac{|\sigma_n^*|^2}{\beta_n} \ . \tag{39}$$

For $\dot{V} \leq 0$, since $p_\sigma = \sigma^{*T} P \sigma^* \geq 0$, the following conditions also have to be satisfied for all n:

$$\sum_{n=1}^{N}(\hat{k}_{h_n} - k_{s_n} f_n)\frac{|\sigma_n^*|}{\beta_n} \geq \sum_{n=1}^{N}\tilde{d}_{0_{M_n}} \tag{40}$$

and

$$\sum_{n=1}^{N} \tilde{k}_{h_n} \frac{|\sigma_n^*|^2}{\beta_n} \geq 0 \ . \tag{41}$$

Ultimately, in the case where $|\sigma_n^*| = \epsilon_n$, one has that $\text{sign}(|\sigma_n^*| - \epsilon_n) = 0$, thus Eq. (38) becomes:

$$\dot{V} \leq -p_\sigma - \sum_{n=1}^{N} \left[\left((\hat{k}_{h_n} - k_{s_n} f_n) \frac{|\sigma_n^*|}{\beta_n} - \tilde{d}_{0_{M_n}} \right) |\sigma_n^*| \right] \ . \tag{42}$$

For $\dot{V} \leq 0$, since $p_\sigma = \sigma^{*T} P \sigma^* \geq 0$, the following condition also have to be satisfied for all n:

$$\sum_{n=1}^{N} (\hat{k}_{h_n} - k_{s_n} f_n) \frac{|\sigma_n^*|}{\beta_n} \geq \sum_{n=1}^{N} \tilde{d}_{0_{M_n}} \ . \tag{43}$$

Thus, in sum, some observations can be inferred. By the adaptation laws as Eqs. (21) and (22), the $\hat{k}_h$ gains are lower bounded by a positive minimum value. It is also seen that when $|\sigma_n^*| > \epsilon_n$, the adaptation law resembles an usual integral-type law, and a sufficient condition for $\dot{V} \leq 0$ is the existence of an ideal value k_{h_n}. However, due to modeling errors, such as parametric uncertainties, external disturbances, measurement noise, and/or non-modeled dynamics, σ_n^* does not remain at zero and may have some oscillations along the time. Consequently, the adaptive gain exhibits the aforementioned parameter drift, which can deviate from its ideal value and possibly to infinity, causing instability problems [48].

In an attempt to avoid this, the term $\text{sign}(|\sigma_n^*| - \epsilon_n)$ was added to adaptation integral law, allowing the gain not only to increase but also decrease. However, note that, since in the cases $|\sigma_n^*| < \epsilon_n$ and $|\sigma_n^*| = \epsilon_n$, the gain $\hat{k}_{h_n}$ decreases and has its update process paused respectively, the conditions Eq. (34), (35), (36), (40), (41) and (43) may not always be met, making $\dot{V}$ sign indefinite in these cases and this insinuates that it is not always possible to conclude on the closed-loop system stability. If $\dot{V} > 0$, V grows and then $|\sigma_n^*|$ can increase and become larger than ϵ_n. Therefore, with the proper conditions, $\dot{V} \leq 0$ can be satisfied, and then, V starts to decrease, denoting an increase-decrease behavior of the adaptive gain dynamics. Note further that conclusions cannot be drawn regarding the convergence of $\hat{k}_{h_n}$ to its ideal value k_{h_n}, indicating that the existence of uncertainties in the estimation of gains causes errors to occur when $t \to \infty$. Even so, they remain bounded, as suggested by the dynamics of adaptive gain.

5 Leader-Follower Trajectory Tracking Control

To avoid collisions between the DWMRs, the distance L_{ij} is measured from the center of the wheels axis of the leader DWMR i to the center of the front of the follower DWMR j. So, L_{ij} and Ψ_{ij} can given as [3]:

$$L_{ij} = \sqrt{L_{ijx}^2 + L_{ijy}^2} \ ; \ \ \Psi_{ij} = \arctan\left(\frac{L_{ijy}}{L_{ijx}}\right) - \theta_i + \pi \ ; \tag{44}$$

$$\begin{aligned} L_{ijx} &= x_{i_{axis}} - x_{j_{front}} = x_i - d_i \cos(\theta_i) - x_j \ ; \\ L_{ijy} &= y_{i_{axis}} - y_{j_{front}} = y_i - d_i \sin(\theta_i) - y_j \ . \end{aligned} \tag{45}$$

The follower DWMR j kinematic model is given as:

$$\dot{q}_j = \begin{bmatrix} \dot{x}_j \\ \dot{y}_j \\ \dot{\theta}_j \end{bmatrix} = \begin{bmatrix} \cos(\theta_j) & -d_j \sin(\theta_j) \\ \sin(\theta_j) & d_j \cos(\theta_j) \\ 0 & 1 \end{bmatrix} \begin{bmatrix} v_{lj} \\ \omega_{aj} \end{bmatrix} \ . \tag{46}$$

Since the follower DWMR j tracks the leader DWMR i, its reference posture vector can be given as [3]:

$$\begin{aligned} x_{jr} &= x_i - d_i \cos(\theta_i) + L_{ijd} \cos(\Psi_{ijd} + \theta_i) \ ; \\ y_{jr} &= y_i - d_i \sin(\theta_i) + L_{ijd} \sin(\Psi_{ijd} + \theta_i) \ ; \\ \theta_{jr} &= \theta_i \ . \end{aligned} \tag{47}$$

Consequently, DWMR j has its posture as [3]:

$$\begin{aligned} x_j &= x_i - d_i \cos(\theta_i) + L_{ij} \cos(\Psi_{ij} + \theta_i) \ ; \\ y_j &= y_i - d_i \sin(\theta_i) + L_{ij} \sin(\Psi_{ij} + \theta_i) \ ; \\ \theta_j &= \theta_j \ . \end{aligned} \tag{48}$$

Seeing Eqs. (47) and (48), considering $\theta_{ij} = \theta_i - \theta_j$, using trigonometric transformations and simplifications, the posture error vector q_{ej} is described by:

$$q_{ej} = \begin{bmatrix} x_{ej} \\ y_{ej} \\ \theta_{ej} \end{bmatrix} = \begin{bmatrix} L_{ijd}\cos(\Psi_{ijd} + \theta_{ij}) - L_{ij}\cos(\Psi_{ij} + \theta_{ij}) \\ L_{ijd}\sin(\Psi_{ijd} + \theta_{ij}) - L_{ij}\sin(\Psi_{ij} + \theta_{ij}) \\ \theta_{jr} - \theta_j \end{bmatrix} . \tag{49}$$

To obtain the error dynamics, it is necessary to calculate the derivatives of L_{ij} and Ψ_{ij}, being the desired values L_{ijd} and Ψ_{ijd} known constants. So, calculating the time derivatives of L_{ijx} and L_{ijy}:

$$\begin{aligned} \dot{L}_{ijx} &= v_{li}\cos(\theta_i) - v_{lj}\cos(\theta_j) + d_j\omega_{aj}\sin(\theta_j) \, ; \\ \dot{L}_{ijy} &= v_{li}\sin(\theta_i) - v_{lj}\sin(\theta_j) + d_j\omega_{aj}\cos(\theta_j) \, . \end{aligned}$$

Considering Eq. (44) and $\zeta_j = \Psi_{ij} + \theta_{ej}$, results in:

$$\begin{aligned} \dot{L}_{ij} &= v_{lj}\cos(\zeta_j) - v_{li}\cos(\Psi_{ij}) + d_j\omega_{aj}\sin(\zeta_j) \, ; \\ \dot{\Psi}_{ij} &= L_{ij}^{-1}\left[v_{li}\sin(\Psi_{ij}) - v_{lj}\sin(\zeta_j) + d_j\omega_{aj}\cos(\zeta_j) - L_{ij}\omega_{ai}\right] . \end{aligned} \tag{50}$$

Due to the separation-bearing formation control objective and the non-slipping constraint [26], the orientations of each DWMR in the formation will not be equal while the formation is turning. For this reason, the orientation of each DWMR cannot be chosen in such a way that $\theta_{jr} = \theta_i$. Thus, from the inverse kinematics, being $\theta^*_{\text{ijr}} = \theta_i - \theta^*_{\text{jr}}$, the auxiliary reference angular velocity is obtained as $\omega^*_{ajr} = \frac{1}{d_j}\left(v_{li}\sin(\theta^*_{\text{ijr}}) + L_{ijd}\omega_{ai}\cos(\Psi_{ijd} + \theta^*_{\text{ijr}})\right)$.

Describing $\dot{q}_{ej}$ by using generic modeling of nonlinear systems and considering the effects of uncertainties and disturbances, one has:

$$\begin{aligned} \dot{q}_{ej} &= A_{0_j}(q_{ej}, t) + B_{0_j}(q_{ej}, t)v_{cj}(t) + d_{b_j}(q_j, t) \\ \begin{bmatrix} \dot{x}_{ej} \\ \dot{y}_{ej} \\ \dot{\theta}^*_{ej} \end{bmatrix} &= \begin{bmatrix} v_{li}\cos(\theta_{ij}) - \omega_{ai}L_{ijd}\sin(\Psi_{ijd} + \theta_{ij}) \\ v_{li}\sin(\theta_{ij}) - \omega_{ai}L_{ijd}\cos(\Psi_{ijd} + \theta_{ij}) \\ \omega^*_{ajr} \end{bmatrix} + \begin{bmatrix} -1 & y_{ej} \\ 0 & -(d_j + x_{ej}) \\ 0 & -1 \end{bmatrix} \begin{bmatrix} v_{lcj} + \tilde{d}_{0_{v_j}} \\ \omega_{acj} + \tilde{d}_{0_{\omega_j}} \end{bmatrix} , \end{aligned} \tag{51}$$

From the posture error dynamics, Eq. (51), with $\theta^*_{\text{ej}} = \theta^*_{\text{jr}} - \theta_j$, the sliding surfaces for the follower DWMR j is defined as:

$$\sigma_j = \begin{bmatrix} \sigma_{v_j} \\ \sigma_{\omega_j} \end{bmatrix} = \begin{bmatrix} \lambda_1 x_{ej} \\ \lambda_2 y_{ej} + \lambda_3 \theta^*_{ej} \end{bmatrix} ; \tag{52}$$

$$\begin{aligned} \sigma^*_{v_j} &= -\lambda_1^2 x_{ej} \, , \\ \sigma^*_{\omega_j} &= \lambda_1^2 y_{ej} x_{ej} - [\lambda_2(d_j + x_{ej}) + \lambda_3](\lambda_2 y_{ej} + \lambda_3 \theta^*_{ej}). \end{aligned} \tag{53}$$

The control laws of the SMC and AIFQSMC for the follower DWMR j are established similarly to Eqs. (11) and (20) respectively, emphasizing that the sliding surfaces are determined by Eqs. (52) and (53), as well as the stability analyses of the closed-loop control systems, which are similar to the stability analyses performed for the leader DWMR i. Considering h followers and proper assumptions as made in [3, 26, 29], the formation stability can be demonstrated utilizing the individual Lyapunov functions and their derivatives as [3]:

$$V_{ij} = (V_i + V_{i_{PD}}) + \sum_{j=1}^{h} (V_j + V_{j_{PD}}) \, , \tag{54}$$

where $V_{i_{PD}}$ and $V_{j_{PD}}$ are determined as in [3] while V_i and V_j are established as Eqs. (10) and (23). Since $V_{j_{PD}} \geq 0$ and $V_j \geq 0$ for all j, and $V_{i_{PD}} \geq 0$ and $V_i \geq 0$, thus, it can be conclude that $V_{ij} \geq 0$.

Differentiating the Eq. (54), one obtains:

$$\dot{V}_{ij} = \left(\dot{V}_i + \dot{V}_{i_{PD}}\right) + \sum_{j=1}^{h} \left(\dot{V}_j + \dot{V}_{j_{PD}}\right) \, , \tag{55}$$

where $\dot{V}_{i_{PD}}$ and $\dot{V}_{j_{PD}}$ are determined as in [3] while $\dot{V}_i$ and $\dot{V}_j$ are established as Eqs. (14) and (25). When $\dot{V}_{j_{PD}} \leq 0$ and $\dot{V}_j \leq 0$ for all j, and $\dot{V}_{i_{PD}} \leq 0$ and $\dot{V}_i \leq 0$, thus, it can be conclude that $\dot{V}_{ij} \leq 0$.

6 Proposed Obstacle Avoidance

Considering the obstacle coordinates (x_a, y_a), as shown in Fig. 4, the relative distance between the DWMR i and the ath obstacle is defined as:

$$d_{ia} = \|l_{ia}\|_2 = \sqrt{(x_a - x_i)^2 + (y_a - y_i)^2} \ , \tag{56}$$

where $l_{ia} = [x_a - x_i \ , \ y_a - y_i]^T$ and $\|\cdot\|_2$ is the Euclidean norm.

Some assumptions can be made as [49–51]:

1. Each mobile robot has an onboard sensing system that can detect the obstacle based on distance measurements;
2. The obstacles are detectable so that their central coordinates are known;
3. An obstacle is considered detected by the DWMR if $d_{ia} \leq D_{det}$, where D_{det} represents the maximum measurement distance of the range sensor attached to the DWMR;
4. The obstacles can be delimited by a circular area with radius r_a;
5. The obstacles are also surrounded by an avoidance area with radius $\overline{R}_d$ that must be larger than the physical obstacles, i.e., $\overline{R}_d > r_a$;
6. In theory, it is considered as a collision occurrence when $d_{ia} \leq r_a$.

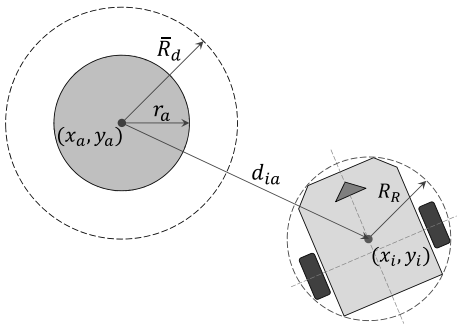

Figure 4: DWMR's relative position to an obstacle.

The constant avoidance area radius $\overline{R}_d$ can be established taking into account the obstacle radius r_a, the robot radius R_R and a safety margin δ_{R_d} as [52]:

$$\overline{R}_d = r_a + R_R + \delta_{R_d}. \tag{57}$$

Some works propose to dynamically modify the radius of the avoidance circle around the obstacle, even if the obstacle dimension does not vary, as in [53–55]. The possibility of expanding the $\overline{R}_d$ value is such that it allows the DWMR trajectory to be affected in advance by the presence of the obstacle, and the collision avoidance task becomes less difficult [56].

In this work, based on the proposal of [55], with the expectation of obtaining a safe and smooth trajectory for the obstacle avoidance, it is introduced a variable avoidance radius R_d, which is adaptively expanded depending on the velocity and direction of movement of the DWMR concerning the obstacle. When the relative distance between the DWMR and the obstacle is greater, there is no priority need to increase the radius value, so more attention should be directed to the trajectory tracking performance. When the relative distance gets smaller, more attention should be paid to safety, which may be suitable for the expansion to be larger. Also, the faster the DWMR is relative to the obstacle, the safer and smoother the movement, and the more appropriate it may be to increase the radius. As this relative velocity decreases, the smaller the expansion can be [55].

Thus, the expansion radius is inversely proportional to the relative distance between the DWMR and the obstacle and directly proportional to the relative velocity. So, the variable avoidance region radius R_d with a self-adaptive expansion radius r_d can be defined as [55]:

$$R_d = \overline{R}_d + r_d \ , \tag{58}$$

$$r_d = \frac{\kappa |v_{ia}|}{\gamma^{\varrho d_{ia}}} \tag{59}$$

where κ is a gain value, ϱ is a parameter used to adjust the denominator value, which is set as $\gamma^{\varrho d_{ia}}$ to make the adaptive expansion radius grow greatly when the relative distance between the DWMR and the obstacle d_{ia} becomes small. Defining the

relative velocity between the DWMR and the obstacle by $v_{l_i} - v_{l_a}$ as in [55], then $v_{ia} = (v_{l_i} - v_{l_a})\cos(\phi)$ is considered the projection of relative velocity over relative distance. Since only static obstacles are considered in this work, $v_{l_a} = 0$. Thus, v_{ia} can be denoted as:

$$v_{ia} = v_{l_i}\cos(\phi) \ , \tag{60}$$

in which

$$\phi = \begin{cases} \theta_i - \theta_{la} & \text{if } \theta_{la} < \theta_i \\ (\theta_i - \theta_{la}) + 2\pi & \text{otherwise} \end{cases} \ , \tag{61}$$

where θ_{la} denotes the angle between the DWMR and the obstacle, given by:

$$\theta_{la} = atan2(y_a - y_i,\ x_a - x_i) \ . \tag{62}$$

It is advisable to limit the avoidance radius R_d so that it does not increase too much, regarding the maximum sensing range of the DWMR, for example. For this, denoting a maximum bound value as $\overline{R}_b$, the radius R_d (Eq. (58)) can be bounded considering it as:

$$R_d = min(\overline{R}_b, \overline{R}_d + r_d) \ . \tag{63}$$

The reactive obstacle avoidance method is based on the one presented in [51], which is considered a switch between a classic backstepping controller and the obstacle avoidance controller. In this work, the structure of the control remains the same, and the reference trajectory is online re-calculated for obstacle avoidance (as usual in some reactive OA approaches [53, 57]), consequently modifying the tracking error dynamics and then influencing the generated sliding surfaces.

The obstacle avoidance mode is activated when the DWMR is tracking the original reference trajectory and the relative distance d_{ia} satisfies the condition:

$$r_a < d_{ia} \leq R_d \ . \tag{64}$$

A vector is established to steer the DWMR in the direction of the vector described as [51]:

$$U_b = l_{ia} - R_d \frac{1}{d_{ia}} l_{ia} \ . \tag{65}$$

Therefore, it can be noted that U_b is a vector pointing towards the obstacle when $d_{ia} > R_d$ and pointing away from the obstacle when $d_{ia} < R_d$, being zero when $d_{ia} = R_d$. It is also expected that the DWMR will drive in a direction parallel to the boundary of the obstacle. So, another vector U_f is established as [51]:

$$U_f = R_f l_{ia} \ ; \tag{66}$$

$$R_f = \begin{bmatrix} \cos(\alpha) & -\sin(\alpha) \\ \sin(\alpha) & \cos(\alpha) \end{bmatrix} . \tag{67}$$

The Eq. (67) determines R_f as a rotation matrix used to transform the vector l_{ia} to the vector U_f, being the value of α defined by:

$$\alpha = \begin{cases} \pi/2, & \theta_i \geq \theta_{la} \\ -\pi/2, & \theta_i < \theta_{la} \end{cases} \ . \tag{68}$$

The Eqs. (62) and (68) are used to determine the fastest direction to the DWMR contour of the obstacle. When $\theta_i > \theta_{la}$, one has $\alpha = \pi/2$ and the vector U_f can be obtained by rotating the vector l_{ia} by α radians counterclockwise. With the value of α remaining constant during obstacle avoidance, the DWMR moves towards its left side to contour the obstacle.

By combining the vectors U_b and U_f, Eqs. (65) and (66), a blending vector is obtained as [51]:

$$U = U_b + U_f = \begin{bmatrix} U_x & U_y \end{bmatrix}^T . \tag{69}$$

Thus, the desired motion direction of the DWMR can be obtained based on the angle of the vector U and the positive direction of the x-axis as:

$$\theta_{r_{OA}} = atan2(U_y,\ U_x) \ , \tag{70}$$

where U_x and U_y are the vector components on the x and y axes respectively.

The reference linear velocity keeps the same in [51], does not changing when going from original trajectory tracking to obstacle avoidance mode. In this work, it was chosen to reduce the linear velocity during the obstacle avoidance as recommended in [49, 58, 59] for safe avoidance.

Similarly to [58], a parameter $0 < \rho_v < 1$ is used to decrease the magnitude of the desired linear velocity when the DWMR avoids an obstacle as:

$$v_{lr_{OA}} = \rho_v v_{lr} \ . \tag{71}$$

Note that if $\rho_v = 1$, the linear velocity remains the same as in normal trajectory tracking. It is worth mentioning that this is a switching mechanism between different reference speeds that can end up generating discontinuities when making the DWMR go slower when avoiding an obstacle and go faster to reach the original velocity. But, for simplicity, it was adopted here.

Considering the inverse kinematics and the reference orientation $\theta_{r_{OA}}$ by Eq. (70), the auxiliary reference angular velocity of Eq. (5), when in the obstacle avoidance mode, is then established as:

$$\omega^*_{ar_{OA}} = -\frac{1}{d_i} v_{lr_{OA}} \sin(\theta^*_{r_{OA}} - \theta_{r_{OA}}) \ . \tag{72}$$

Thereby, it can be seen that obstacle avoidance occurs mainly due to a modification of the original desired DWMR's orientation, with a just reduction in the linear velocity. So, basically, for a better understanding, $q_{r,tt} = [x_{r,tt}\ y_{r,tt}\ \theta_{r,tt}]^T$ and $v_{r,tt} = [v_{lr,tt}\ \omega_{ar,tt}]^T$ can be denoted as the original trajectory tracking reference posture and velocities respectively, and $q_{r,oa} = [x_{r,oa}\ y_{r,oa}\ \theta_{r,oa}]^T$ and $v_{r,oa} = [v_{lr,oa}\ \omega_{ar,oa}]^T$ as the reference posture and velocities in the obstacle avoidance mode respectively. Only one mode is active at a time, that is, the reference motion (q_r, v_r) will assume only ($q_{r,tt}$, $v_{r,tt}$) or ($q_{r,oa}$, $v_{r,oa}$). If the condition determined by the Eq. (64) is met, obstacle avoidance mode is activated, otherwise the desired motion is prescribed by the original trajectory tracking. In this way, in obstacle avoidance mode, the posture error is described similarly as Eq. (4) with $q_r = q_{r,oa}$, for which it is considered Eq. (70), and the error dynamics is similar to Eq. (6) considering Eq. (72), based on which the sliding surfaces in obstacle avoidance mode are obtained similarly to the process for Eqs. (7) and (9). With these sliding surfaces, as the control structure remains the same, the SMC and AIFQSMC control laws are established similarly to Eqs. (11) and (20) respectively. A variable c can be established to represent the obstacle avoidance mode state, which can be 1 if it is active and 0 otherwise.

So, a total Lyapunov function for the leader kinematic controllers can be defined as:

$$V_t = (1 - c)V_{tt} + cV_{oa} \tag{73}$$

where V_{tt} and V_{oa} are set by Eqs. (10) and (23).

The time derivative of Eq. (73) is denoted as:

$$\dot{V}_t = (1 - c)\dot{V}_{tt} + c\dot{V}_{oa} \tag{74}$$

where similarly $\dot{V}_{tt}$ and $\dot{V}_{oa}$ are established as Eqs. (14) and (26) for SMC and AIFQSMC respectively.

Accordingly, this means that, depending on which mode is active, $V_t = V_{tt}$ or $V_t = V_{oa}$, and $\dot{V}_t = \dot{V}_{tt}$ or $\dot{V}_t = \dot{V}_{oa}$, being the proofs that $V_{tt} > 0$, $V_{oa} > 0$, $\dot{V}_{tt} \leq 0$ and $\dot{V}_{oa} \leq 0$ demonstrated similarly in the stability analyses performed in the Sections 3.2 and 4.2. Note also that the convergence of the original to the obstacle avoidance reference trajectory or vice versa is not treated, assuming smoothness and convergence of the DWMR's orientation to near surroundings of reference orientation. Thus, updating the reference can lead to a temporary degeneration of the tracking performance, which can be seen as a disturbance effect. So, it is up to the proposed robust controller to handle the tracking errors resulting from obstacle avoidance.

7 Implementation results

Simulation results using Matlab/Simulink software (version R2020b), with the total simulation time of 200s and the Dormand-Prince solver, are obtained for the trajectory tracking formation control, for the leader DWMR i and the follower DWMRs j, the embedded PD control as dynamic controller, with control law defined by Eq. (2), which can be described as

$$\tau \ = \ \overline{E}(q)^{-1} \left(k_d \dot{v}_e + k_p v_e\right) \tag{75}$$

in time domain, integrated with the kinematic controllers SMC and AIFQSMC, with control law established as Eqs. (11) and (20) respectively. It is pointed out that when not specified some considerations for choosing parameters are described in the previous sections), constant gains can be optimized using the tools *Simulink Design Optimization* and *Response Optimization* of Matlab/Simulink software and with a manual fine-tuning if necessary as described in [60].

It is important to underline that it was considered a homogenous system formation architecture, so the same gain values should be considered for all robots. The same values were adopted for the common parameters for the comparative study between the different controllers.

The simulation scenario is considered a configuration model with the limitations of the PowerBot DWMR, a closed platform with internal PD controllers that tracks input variables v_e and ω_e with a sampling time of 5 ms. Furthermore, some modifications to the DWMR configuration model are necessary because the internal PD control signals generate generalized forces acting at the DWMR's center of inertia and must be converted into torques on the wheels to be taken as control inputs in the present configuration model. So, the signals of the PD controllers are premultiplied by the matrix T_v^{-1}, which relates torques to the wheels with generalized torques, given as [28]: $T_v^{-1} = \left[\frac{1}{r}\ \ \frac{b}{r};\ \frac{1}{r}\ \ \frac{-b}{r}\right]$, where $2b$ is the width of the PowerBot DWMR. Moreover,

to simulate the behavior of the PowerBot DWMR, the configuration state-space model with the actuator dynamics representing the structural uncertainty is considered similarly to [28]. The specifications and parameters in nominal values of the PowerBot DWMR can also be seen in [28] or in the manufacturer's manual.

The gains of the PD dynamic controller are adjusted as $k_{p_v} = 40$, $k_{p_\omega} = 40$, $k_{d_v} = 20$, $k_{d_\omega} = 20$, $N_v = 10$ and $N_\omega = 10$ as indicated by the manufacturer. The parameters N_v and N_ω are set to 10 to ensure good response time of the internal loop against the neglected dynamics and avoid chattering [28, 30].

An eight-shape trajectory, starting in a counterclockwise direction, was adopted as reference trajectory. In view of the acceleration and deceleration along it, it has a complexity defined by the changes in velocities, with linear velocity varying between 0.33 m/s and 1.05 m/s, and the angular velocity, -0.18 rad/s and 0.18 rad/s. It is formulated as [3]:

$$\dot{q}_r = \begin{bmatrix} \dot{x}_r \\ \dot{y}_r \\ \dot{\theta}_r \end{bmatrix} = \begin{bmatrix} \left(30\, sin\left(\left(t + \frac{200}{4}\right)\frac{2\pi}{200}\right)\frac{2\pi}{200}\right)/2 \\ -30cos\left(2\left(t + \frac{200}{4}\right)\frac{2\pi}{200}\right)\frac{2\pi}{200} \\ \frac{\ddot{y}_r\dot{x}_r - \ddot{x}_r\dot{y}_r}{\dot{x}_r^2 + \dot{y}_r^2} \end{bmatrix};$$

$$v_r = \begin{bmatrix} v_{lr} \\ \omega_{ar} \end{bmatrix} = \begin{bmatrix} \sqrt{\dot{x}_r^2 + \dot{y}_r^2} \\ \dot{\theta}_r \end{bmatrix}. \tag{76}$$

Table 4 presents the initial conditions and the values of d. For all DWMRs, the gains of the SMC are $p_v = p_\omega = g_v = g_\omega = 0.1$ (as minimum values), $\lambda_1 = 0.5$, $\lambda_2 = 0.3$ and $\lambda_3 = 0.7$.

The desired separation-bearing values L_{ijd} and Ψ_{ijd} are defined as shown in Table 5.

For the FIS used to compute the function $f(\cdot)$, the MFs can be graphically represented by Figs. 5a, 5b and 6, being the parameters given in Tables 6 and 7, where α_1 and α_3 are the "feet" of the triangle, and α_2 locates the peak. For the boundary layer thickness FIS, the MFs can be illustrated by Fig. 7 with the parameters given in Table 8.

Since the nonlinear function $f(\cdot)$ can assume negative and positive values, the output MF values of the FIS to compute it can be obtained by taking into account the following considerations. Given that: f is computed by a Mamdani FIS, it is bounded by a minimum negative value f_{min} and a maximum positive value f_{max}, the gain $\hat{k}_h$ is adaptive with a minimum positive value $\overline{k}_h$, and also that k_s is constant gain, defining a minimum value $\hat{G}_{AIS(min)}$ for $\hat{G}_{AIS}$ (such that $0 < \hat{G}_{AIS(min)} < \overline{k}_h$), to avoid $\hat{G}_{AIS} = \hat{k}_h - k_s f < 0$, the choice of f_{max} is such that:

$$\begin{aligned} \hat{G}_{AIS(min)} &= \overline{k}_h - k_s f_{max} \\ f_{max} &= (\overline{k}_h - \hat{G}_{AIS(min)})/k_s \ . \end{aligned}$$

Therefore, the peak value (α_2) of the *PM* triangular MF for the output $f(\cdot)$ (Table 7 and Fig. 6) need to be relatad to this value, f_{max}. There would be no restriction for the value of f_{min} (related to the peak of the *NB* MF of the FIS output), and its choice would depend on the controller performance since it is related to the stimulus reaction (maximum containment of the suppression effect) by adding $k_s f$ to the value of $\hat{k}_h$. Here, $f_{min} = -1$, thus, $\hat{k}_h$ can be increased by a full value or a percentage of k_s depending on the negative value of $f(\cdot)$.

Table 4: Initial posture and parameter d of the DWMRs.

	x_0	y_0	θ_0	d
Reference	0	0	$\pi/2$	0
Leader	-1	1	0	0.1
Follower 1	-3.5	3	0	0.4
Follower 2	-3	-1	0	0.4

Table 5: Values of Ψ_{ijd} and L_{ijd} for followers.

	Ψ_{ijd}	L_{ijd}
Follower 1	$(3/4)\pi$ rad	1.25 m
Follower 2	$-(3/4)\pi$ rad	1.25 m

For the AIFQSMC, it was established that $\hat{k}_{h_n}(t=0) = \overline{k}_{h_n} = 0.1$, as a minimum positive gain value, $\epsilon_v = \epsilon_\omega = 0.05$, $k_{s_v} = 0.55$ and $k_{s_\omega} = 0.55$ for all DWMRs. The values of Γ_h are shown in Table 9.

To verify the compensatory characteristics behavior of the kinematic controllers in a disturbed case, simulations are performed considering load variations of mass and moment of inertia (in the time range of 40 to 160 s), as well as unmodeled dynamics

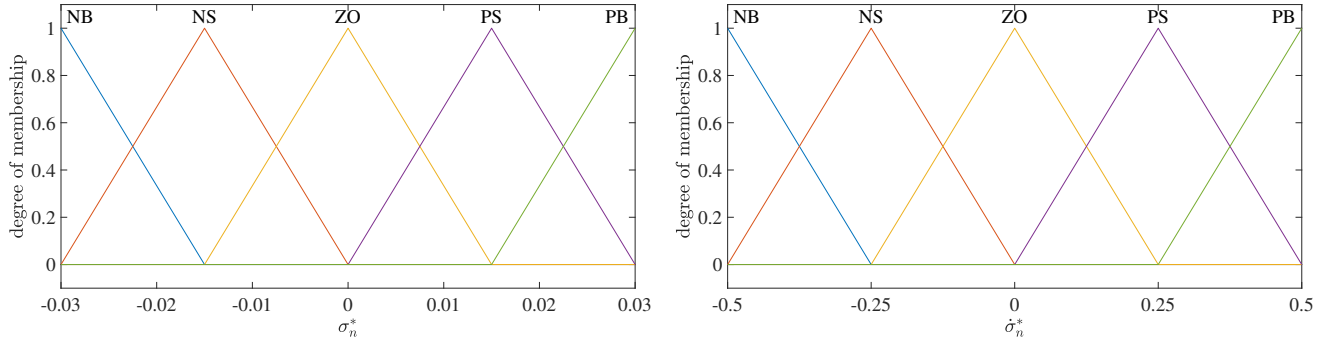

(a) Triangular-shaped MFs for input σ^* (AIS).

(b) Triangular-shaped MFs for input $\dot{\sigma}^*$ (AIS).

Figure 5: Triangular-shaped MFs for inputs σ^* and $\dot{\sigma}^*$ (AIS).

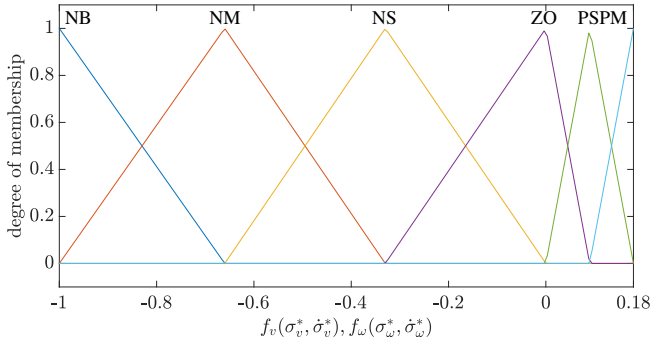

Figure 6: Triangular-shaped MFs for output $f_n(\cdot)$ (AIS).

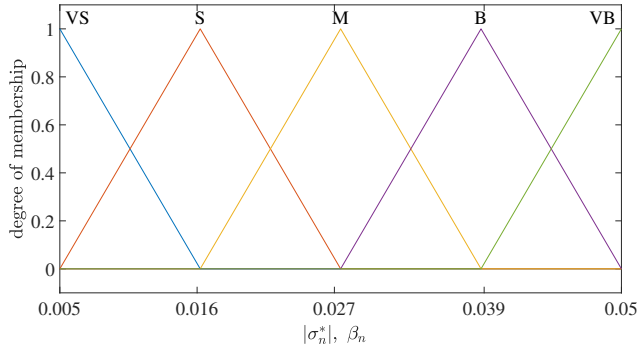

Figure 7: Triangular-shaped MFs for input and output (BL).

Table 6: Parameters of MFs for input σ^* and $\dot{\sigma}^*$.

	σ^*			$\dot{\sigma}^*$		
	α_1	α_2	α_3	α_1	α_2	α_3
NB	$-\infty$	-0.030	-0.015	$-\infty$	-0.50	-0.25
NS	-0.030	-0.015	0.000	-0.50	-0.25	0.00
ZO	-0.015	0.000	0.015	-0.25	0.00	0.25
PS	0.000	0.015	0.030	0.00	0.25	0.50
PB	0.015	0.030	∞	0.25	0.50	∞

introduced in the form of friction (during the entire simulation time). External disturbances with unknown upper bounds are also applied on the system at different time intervals (time-varying sinusoidal form at 3 to 20 s and 100 to 120s; constant signal at 50 to 70 s and 150 to 170 s). These uncertainties and disturbances are similar to those considered in [27].

For the case with obstacle avoidance, it was considered: $\rho_v = 0.1$, obstacles of radius $r_a = 0.5$ m, the DWMR's radius approximately $R_R = 0.56$ m, as can be seen in the manufacturer manual, and a security margin $\delta_{R_d} = 1.7m$, considering the desired separation plus a deviation (1.25 + 0.45). The parameters for the variable avoidance radius R_d are shown in Table 10. The obstacle coordinates were established similarly to [61] as shown in Table 11.

To measure the chattering level, $|\dot{v}_c|$ is adopted [43]. As commonly used in the literature, the root mean square errors (RMSE)

Table 7: Parameters of MFs for output $f(\cdot)$.

	f_n		
	α_1	α_2	α_3
NB	$-\infty$	-1.00	-0.66
NM	-1.00	-0.66	-0.33
NS	-0.66	-0.33	0.00
ZO	-0.33	0.00	0.09
PS	0.00	0.09	0.18
PM	0.09	0.18	∞

Table 8: Parameters of MFs for Fuzzy BL.

	$\lvert\sigma_n^*\rvert,\ \beta_n$		
	α_1	α_2	α_3
VS	10^{-6}	0.0050	0.0162
S	0.0050	0.0162	0.0275
M	0.0162	0.0275	0.0387
B	0.0275	0.0387	0.0500
VB	0.0387	0.0500	∞

Table 9: Values of $\overline{k}_h$ and Γ_h.

	$\overline{k}_{h_v}$	Γ_{h_v}	$\overline{k}_{h_\omega}$	Γ_{h_ω}
Leader	0.1	0.15	0.1	0.40
Follower 1	0.1	0.15	0.1	0.40
Follower 2	0.1	0.15	0.1	0.40

Table 10: Parameters for the variable avoidance region radius R_d.

$\overline{R}_d$ [m]	$\overline{R}_b$ [m]	κ	γ	ϱ
2.76	5.00	5.00	2.00	1.00

Table 11: Obstacles coordinates.

	Obstacle 1	Obstacle 2	Obstacle 3
x_a	0.00	8.00	-14.50
y_a	15.50	-4.25	-11.25

is used as a performance evaluation method, being given by $RMSE(x) = \left[\frac{1}{T}\sum x^2\right]^{1/2}$, where T is the number of samples and $x(k)$ is the value of the *k*-th sample [27, 28].

Table 12: RMSE values in a disturbed case.

		$RMSE(x_e)$	$RMSE(y_e)$	$RMSE(\theta_e)$
Leader	SMC	3.2309	3.4591	4.0197
	AIFQSMC	0.5399	0.6988	**0.2327**
	FCAFSMC	**0.4519**	**0.5694**	0.2546
Follower 1	SMC	0.8302	2.3546	0.4170
	AIFQSMC	**0.1298**	**0.1340**	**0.0318**
	FCAFSMC	0.1806	0.1883	0.0528
Follower 2	SMC	0.7973	1.9537	0.4404
	AIFQSMC	**0.1008**	**0.1114**	**0.0206**
	FCAFSMC	0.1456	0.1693	0.0427

7.1 Simulation results for SMC

Results for SMC are illustrated by Figs. 8a to 12b. The static obstacles distributed along the trajectory according to Table 11 can be seen in the first figure (Fig. 8a), which also readily shows that there were troubles in tracking by the leader robot and

information by the followers. Besides that, Fig. 8b shows high levels of measured chattering. The robustness is affected because, when the gains are not enough, there is no compensation for auxiliary velocity tracking errors (see Figs. 9a, 9b, 10a). Separation and bearing errors are also affected (see Fig. 10b) and the control system has difficulty finding stability (see Figs. 11a, 11b, 12a, 12b), despite the OA strategy acting in the collisions prevention for the leader.

This leads to larger RMSE values (see Table 12). Thus, the effectiveness in terms of robustness against uncertainties and disturbances depends on an adequate choice of the gain values, and hence *a priori* knowledge of the bounds of the disturbances is required to ensure the compensatory effect of the SMC.

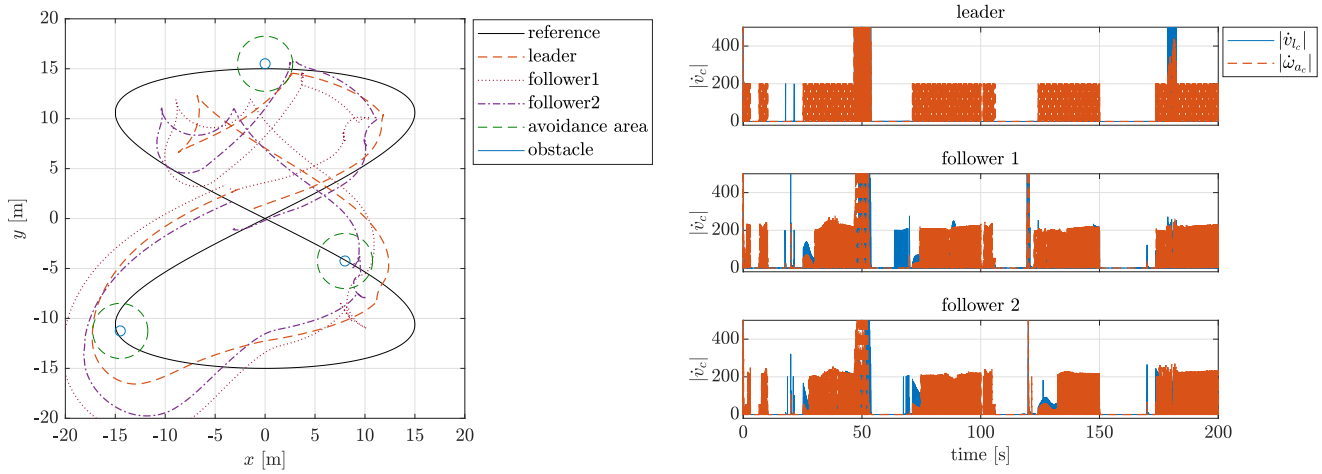

(a) Trajectory tracking, formation, OA.

(b) Chattering measure.

Figure 8: Trajectory tracking, formation, OA, and chattering measure (SMC).

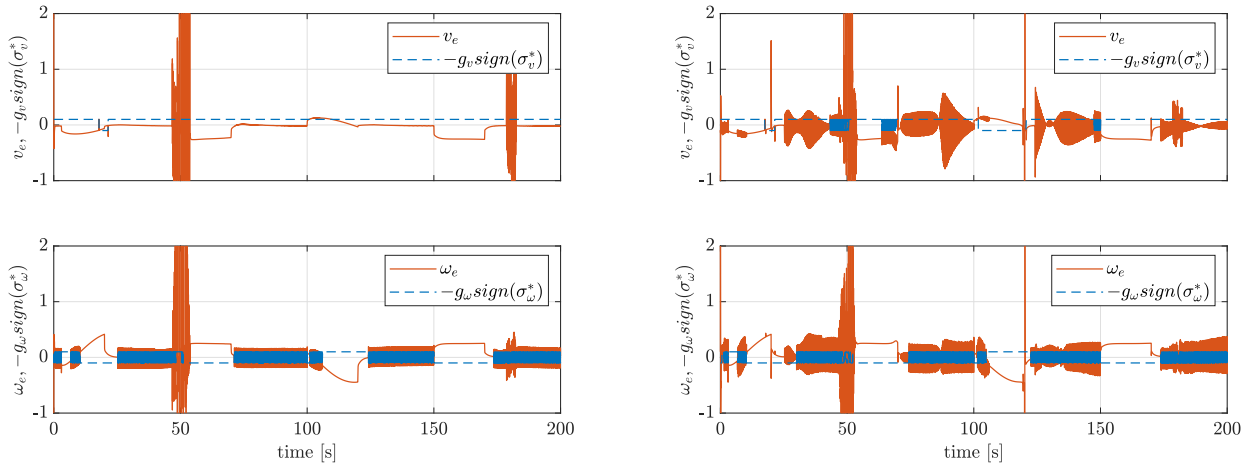

(a) Leader: Auxiliary velocity tracking errors and compensations.

(b) Follower 1: Auxiliary velocity tracking errors and compensations.

Figure 9: Auxiliary velocity tracking errors and compensations - Leader and Follower 1 (SMC).

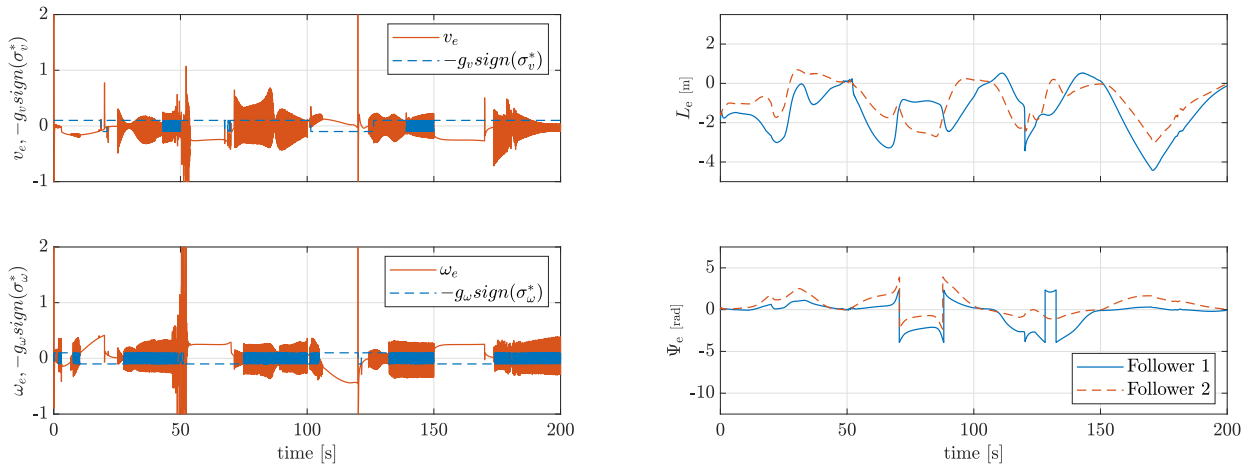

(a) Follower 2: Auxiliary velocity tracking errors and compensations.

(b) Separation and bearing errors.

Figure 10: Auxiliary velocity tracking errors and compensations - Follower 2 - and separation-bearing errors (SMC).

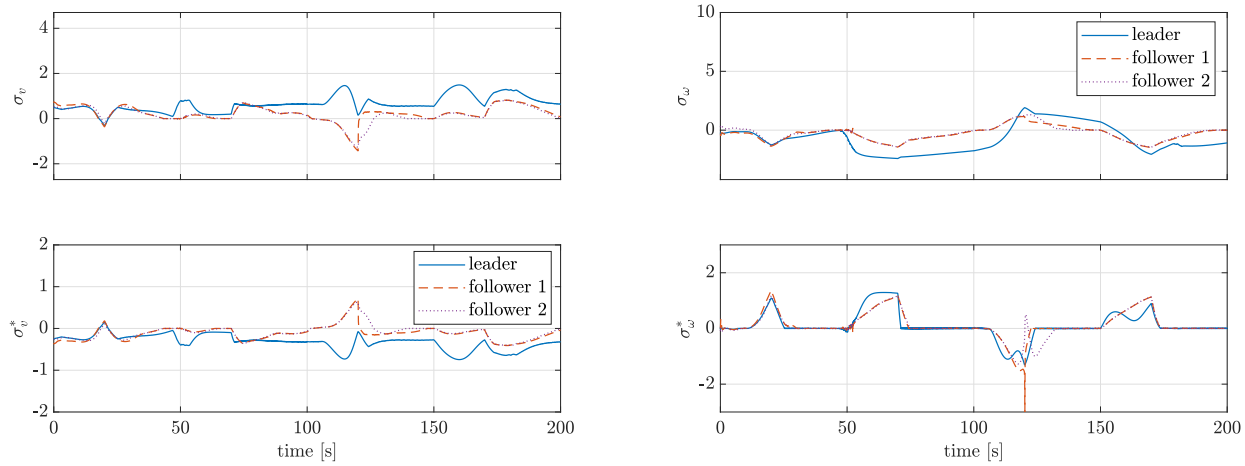

(a) Sliding surfaces σ_v and σ_v^*.

(b) Sliding surfaces σ_ω and σ_ω^*.

Figure 11: Sliding surfaces σ_n and σ_n^* (SMC).

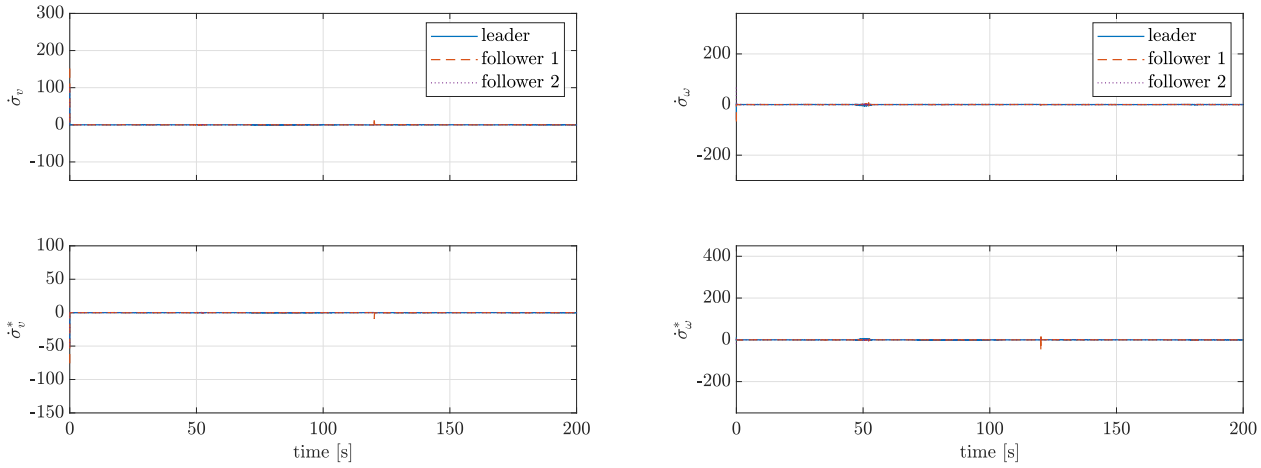

(a) Derivatives of sliding surfaces σ_v and σ_v^*.

(b) Derivatives of sliding surfaces σ_ω and σ_ω^*.

Figure 12: Derivatives of sliding surfaces σ_n and σ_n^* (SMC).

7.2 Simulation results for AIFQSMC

The Figs. 13a to 23b show the results for AIFQSMC. By Fig. 13a, it can be seen that the DWMRs could get around the obstacles. A smoother behavior than the SMC is observed in Fig. 13b. The obstacle avoidance is established by the blending vectors displayed in Fig. 14a. When the obstacle avoidance mode is activated, new reference posture $\theta_r = \theta_{r_{OA}}$ is generated to steer the DWMR around the obstacles (see Fig. 14b). The switching between reference in the original trajectory tracking mode ($q_{r,tt}$, $v_{r,tt}$) and in the obstacle avoidance mode ($q_{r,oa}$, $v_{r,oa}$) can be lead to a tracking performance degeneration as the DWMR modifies its orientation to achieve the new desired motion. So, since obstacle avoidance is applied for the leader DWMR, greater errors were obtained compared to the errors for the follower DWMRs. Table 12 exhibits the obtained RMSE values for the AIFQSMC controller in a disturbed case with obstacle avoidance. For visualization, the avoidance area is shown by a circle of constant radius $\overline{R}_d$ in the Fig. 13a. The behavior of the variable radius R_d is seen more clearly in Figs. 15a, 15b and 16a, by which it can be noted that the expansion tends to increase as the DWMR starts to approach or move away from the obstacle, making the motion smoother. By Fig. 16b, it is observable that the collision does not occur seeing the relative distance between the leader DWMR and the obstacles, as well as for the followers (Figs. 17a and 17b). Note further that the deviations of obstacles coincide with the incidence of the disturbances (at the beginning, middle, and end of the disturbance effect for each obstacle, respectively) as can be seen in Figs. 18a, 18b, 19a. Making the separation-bearing errors, the sliding surfaces and their derivatives reach the zero surroundings (Figs. 19b, 20a, 20b, 21a, 21b), the controller was able to adapt to overcome the arising errors and prevent the system from instabilizing as seen in Figs. 22a, 22b, 23a and 23b.

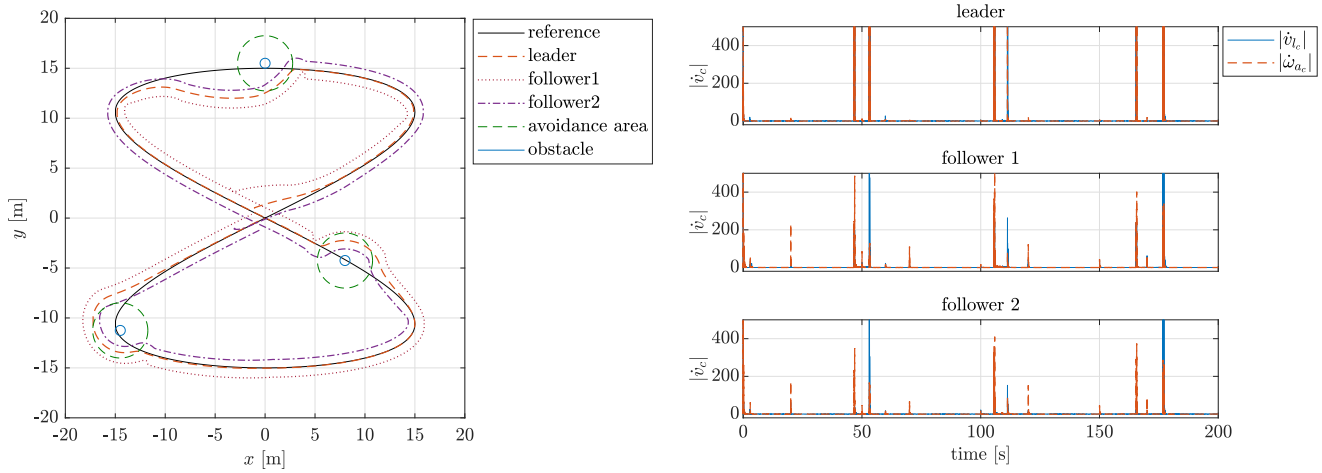

(a) Trajectory tracking, formation, OA.

(b) Chattering measure.

Figure 13: Trajectory tracking, formation, OA, and chattering measure (AIFQSMC).

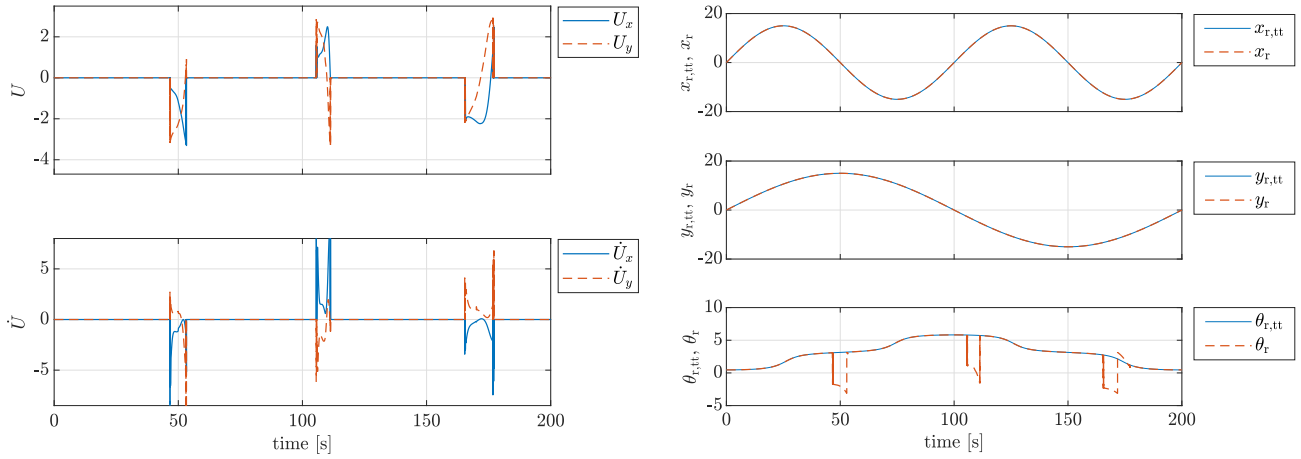

(a) OA blending vectors.

(b) OA reference posture.

Figure 14: OA blending vectors, reference posture in original trajectory tracking and obstacle avoidance mode (AIFQSMC).

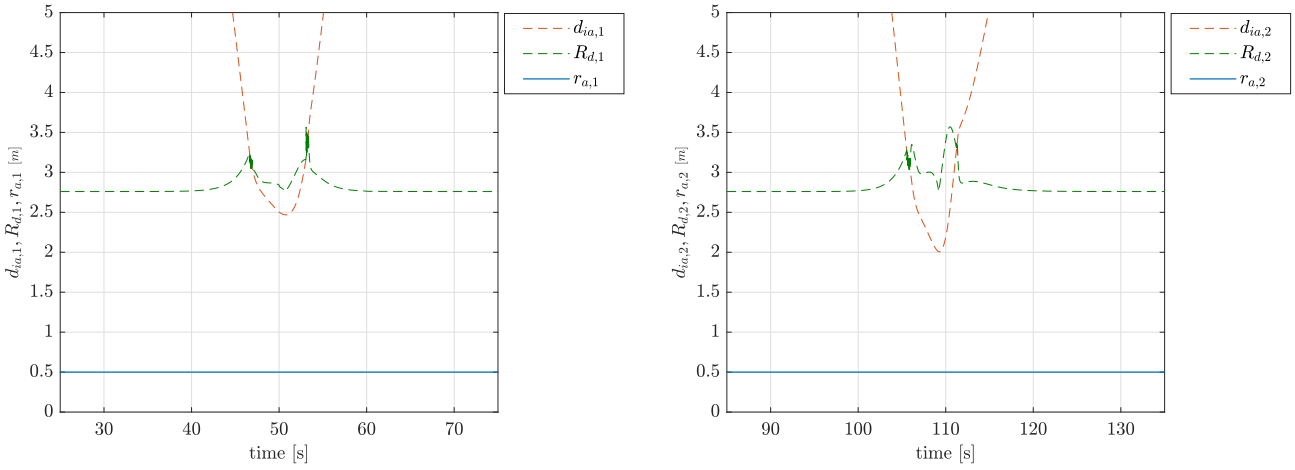

(a) $R_{d,1}$ (zoomed plot). (b) $R_{d,2}$ (zoomed plot).

Figure 15: Variable radii $R_{d,1}$ and $R_{d,2}$ (AIFQSMC).

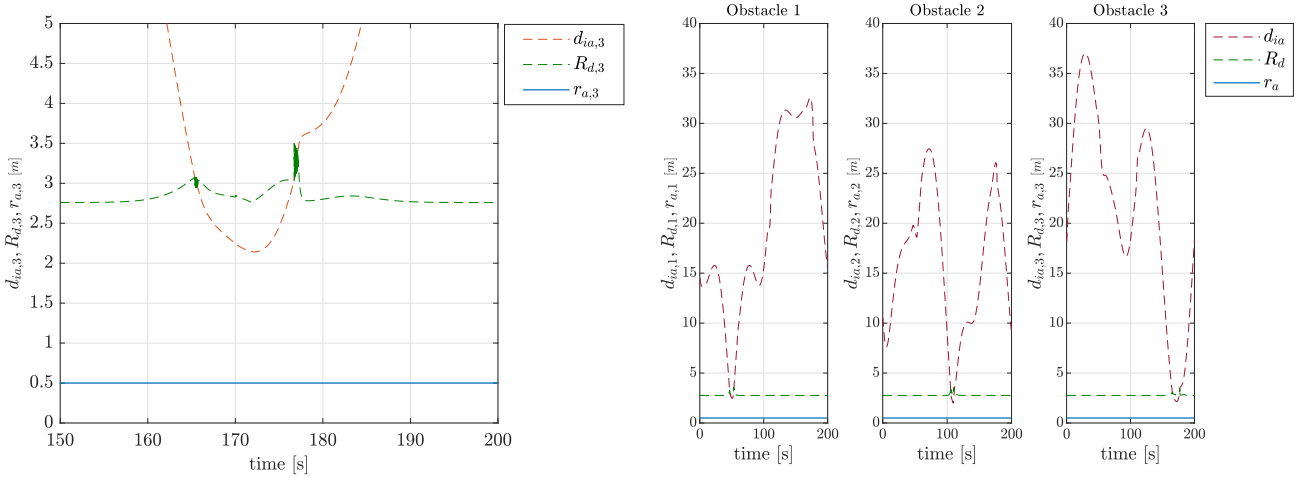

(a) $R_{d,3}$ (zoomed plot). (b) Relative distance between the leader DWMR and the obstacles.

Figure 16: Variable radius $R_{d,3}$ and relative distance between the leader DWMR and the obstacles (AIFQSMC).

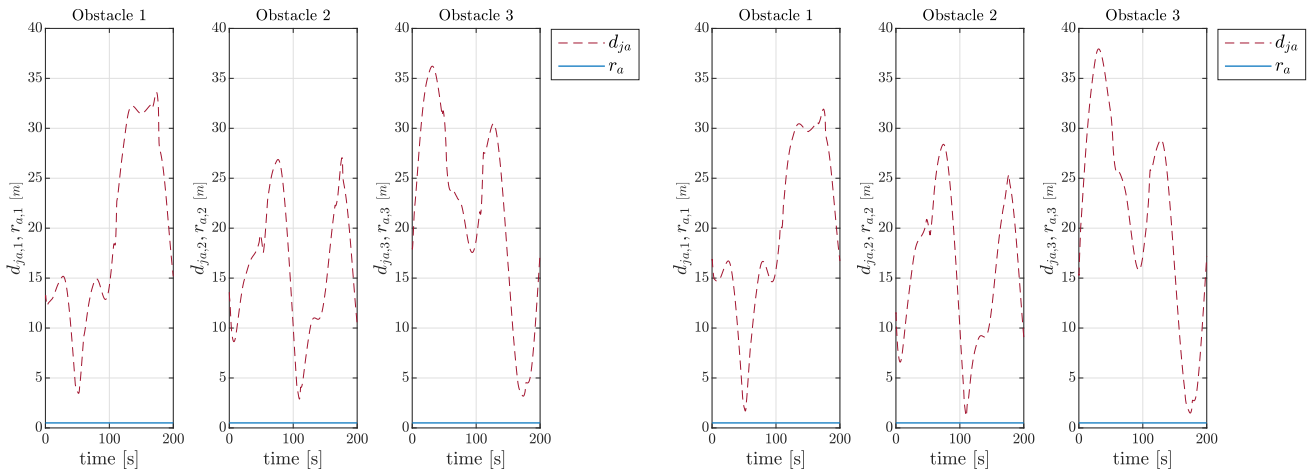

(a) Relative distance between the follower 1 DWMR and the obstacles. (b) Relative distance between the follower 2 DWMR and the obstacles.

Figure 17: Relative distance between the followers DWMRs and the obstacles (AIFQSMC).

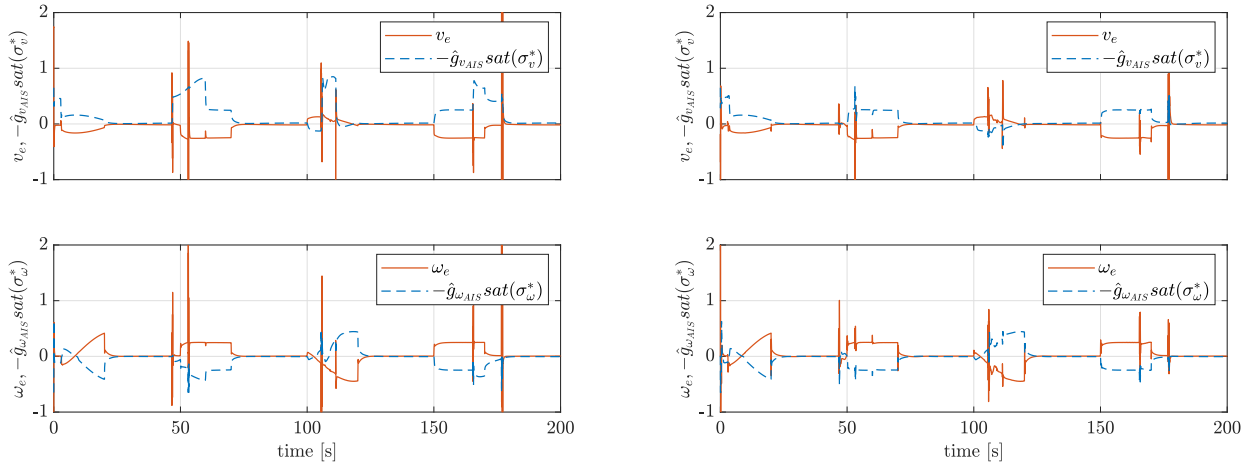

(a) Leader: Auxiliary velocity tracking errors and compensations.

(b) Follower 1: Auxiliary velocity tracking errors and compensations.

Figure 18: Auxiliary velocity tracking errors and compensations - Leader and Follower 1 (AIFQSMC).

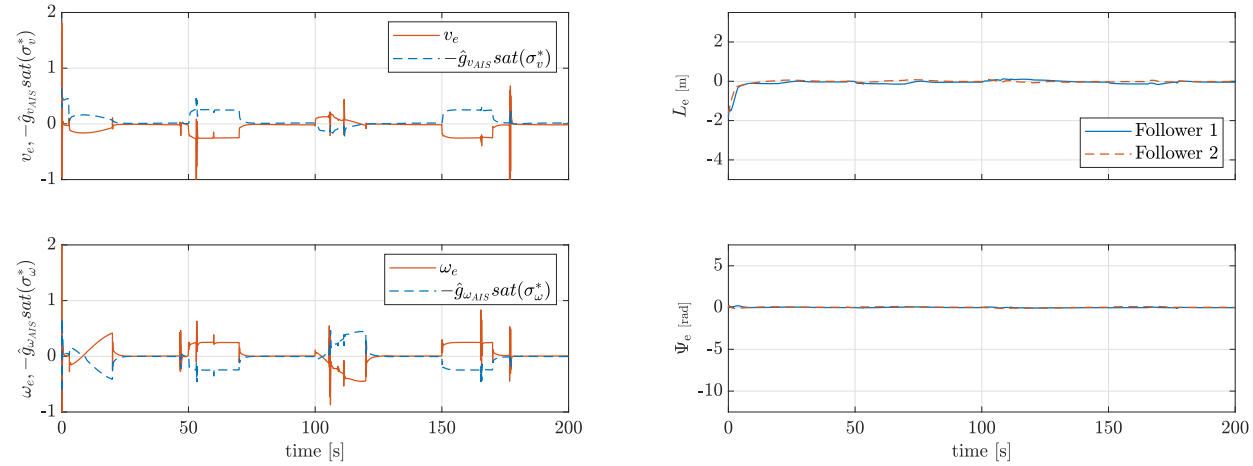

(a) Follower 2: Auxiliary velocity tracking errors and compensations.

(b) Separation and bearing errors.

Figure 19: Auxiliary velocity tracking errors and compensations - Follower 2 - and separation-bearing errors (AIFQSMC).

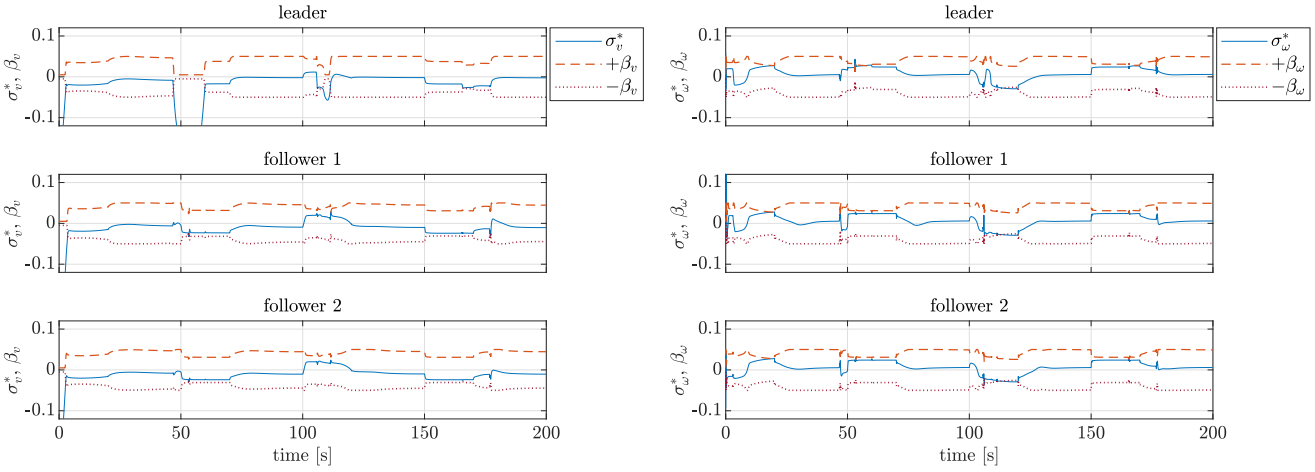

(a) σ_v^* and β_v.

(b) σ_ω^* and β_ω.

Figure 20: σ_n^*-trajectories with time-varying boundary layer β_n (zoomed plot) (AIFQSMC).

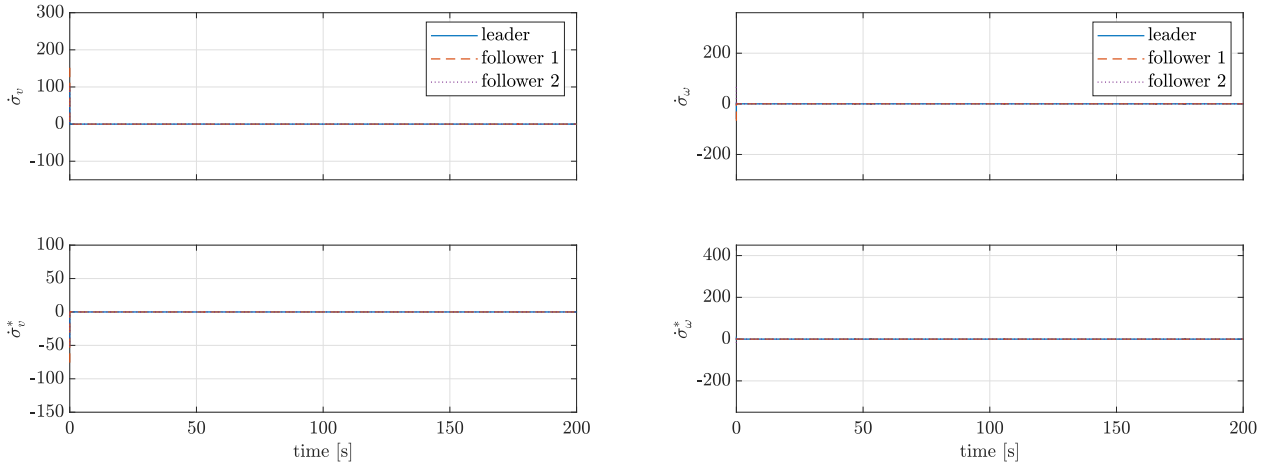

(a) $\dot{\sigma}_v$ and $\dot{\sigma}_v^*$. (b) $\dot{\sigma}_\omega$ and $\dot{\sigma}_\omega^*$.

Figure 21: Derivatives of sliding surfaces (AIFQSMC).

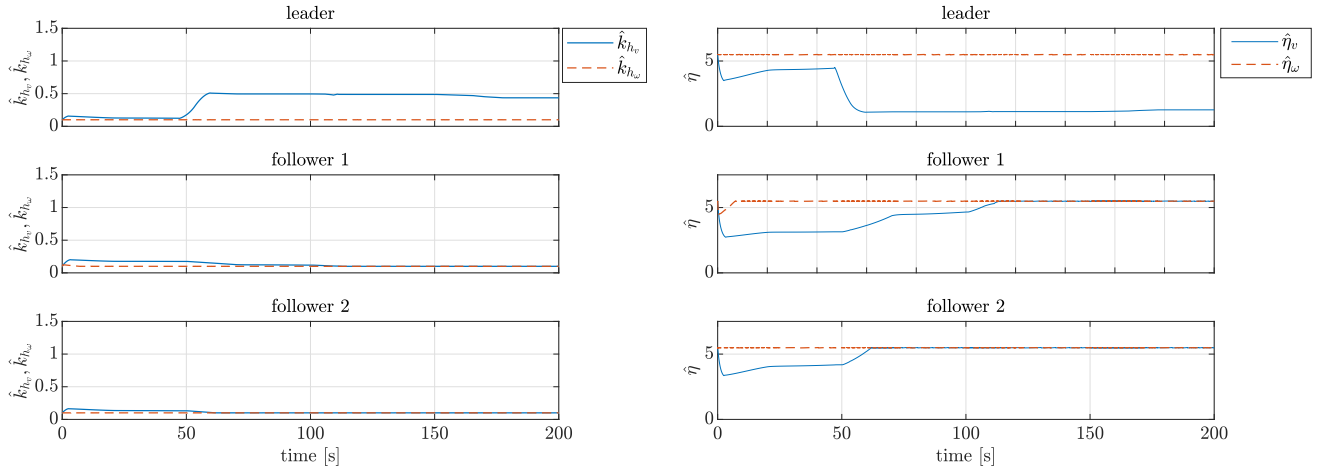

(a) Adaptive gains $\hat{k}_h$. (b) Time-varying parameter $\hat{\eta}$.

Figure 22: Adaptive gains $\hat{k}_h$ and $\hat{\eta}$ (AIFQSMC).

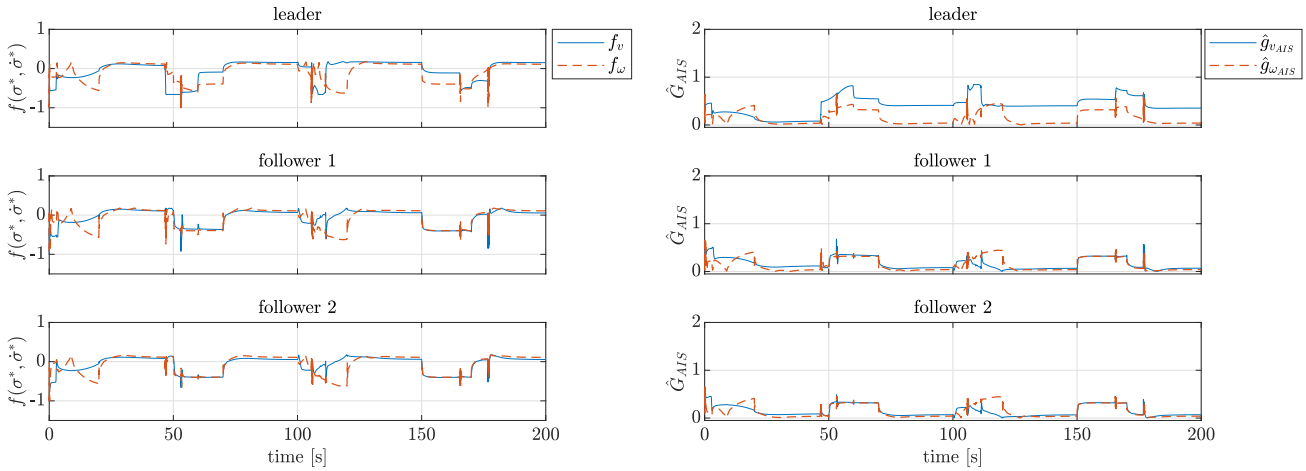

(a) AIS function $f(\sigma^*, \dot{\sigma}^*)$. (b) AIS gain $\hat{G}_{AIS}$.

Figure 23: AIS function $f(\sigma^*, \dot{\sigma}^*)$ and gain $\hat{G}_{AIS}$ (AIFQSMC).

7.3 Simulation results for FCAFSMC

Comparisons with another approach are performed, considering the embedded PD dynamic control integrated with the Formation Controller - Adaptive Fuzzy Sliding Mode Control (FCAFSMC) proposed in [3]. In this adaptive controller, the discontinuous sliding mode portion, $Gsign(\sigma^*)$, is replaced by a fuzzy gain $\hat{F}(\sigma^*) = \hat{C}^T\xi(\sigma^*)$, i.e.:

$$v_c = -B_{0_\sigma}^{-1}A_{0_\sigma} - \hat{F}(\sigma^*) - P\sigma^*, \tag{77}$$

where $\hat{C}$ is the online updated consequences vector and $\xi(\sigma^*)$ is the rule weights vector. The adaptation law for $\hat{C}$ is given by [3]:

$$\dot{\hat{C}} = \sigma^*\xi(\sigma^*). \tag{78}$$

It is important to point out that the rule base, the triangular-shaped membership functions and their parameters, as well as the stability analysis and other details of the FCAFSMC, are described in [3]. Differently of [3], the FCAFSMC was employed taking into account the same system modeling based on inverse kinematics, the same values for parameters in common, the same uncertainties and disturbances as well as the same obstacle avoidance strategy adopted for the AIFQSMC.

The RMSE values are shown in Table 12 and results, in the Figs. 24a to 28b, from which it can be observed satisfactory performance for the trajectory tracking and formation control. The FCAFSMC had smaller errors in x and y for the leader, but in general the errors were equivalent to the AIFQSMC, the obstacle avoidance was completed and the movements were smooth.

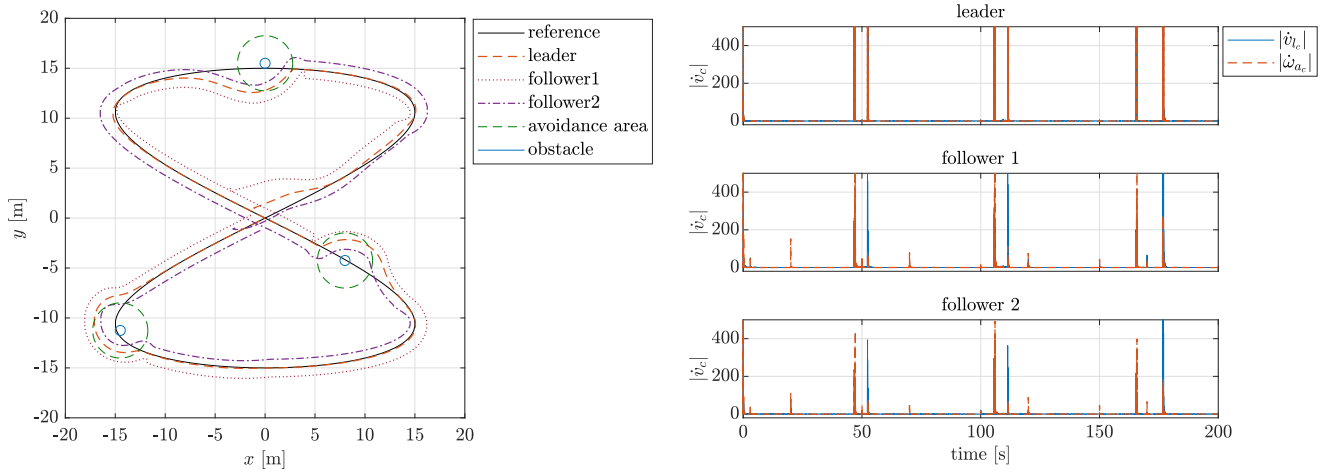

(a) Trajectory tracking, formation, OA.

(b) Chattering measure.

Figure 24: Trajectory tracking, formation, OA, and chattering measure (FCAFSMC).

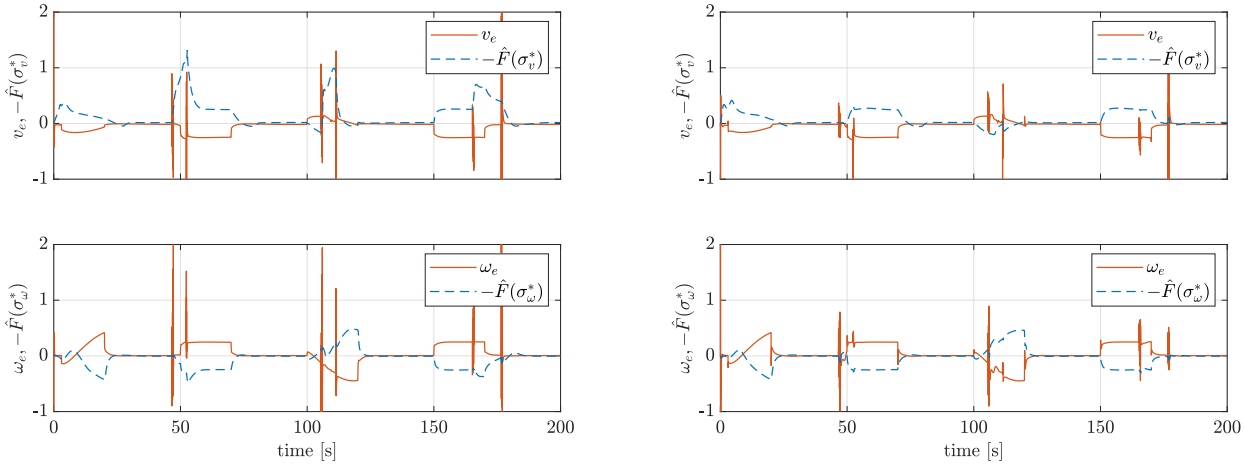

(a) Leader: Auxiliary velocity tracking errors and compensations.

(b) Follower 1: Auxiliary velocity tracking errors and compensations.

Figure 25: Auxiliary velocity tracking errors and compensations - Leader and Follower 1 (FCAFSMC).

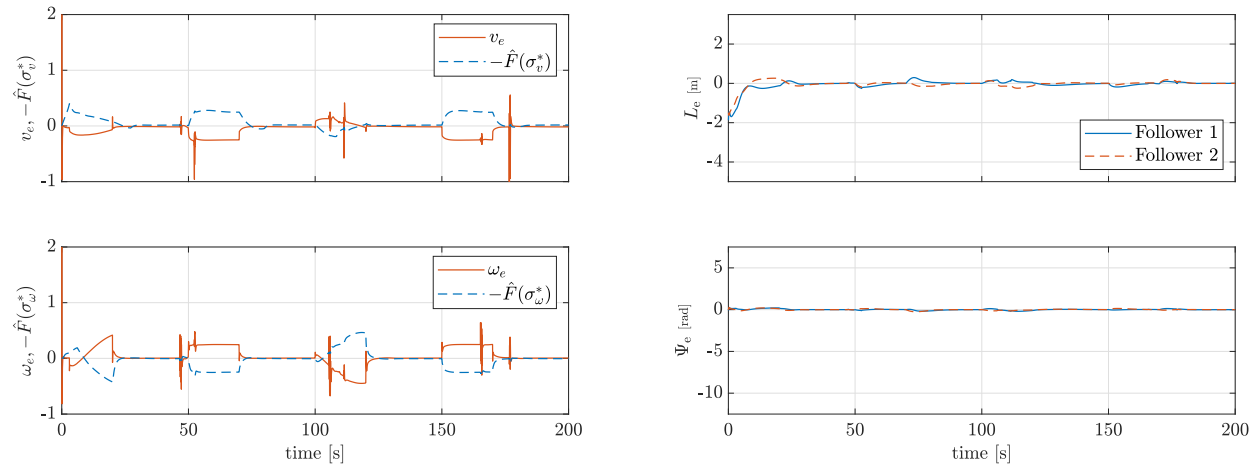

(a) Follower 2: Auxiliary velocity tracking errors and compensations.

(b) Separation and bearing errors.

Figure 26: Auxiliary velocity tracking errors and compensations - Follower 2 - and separation-bearing errors (FCAFSMC).

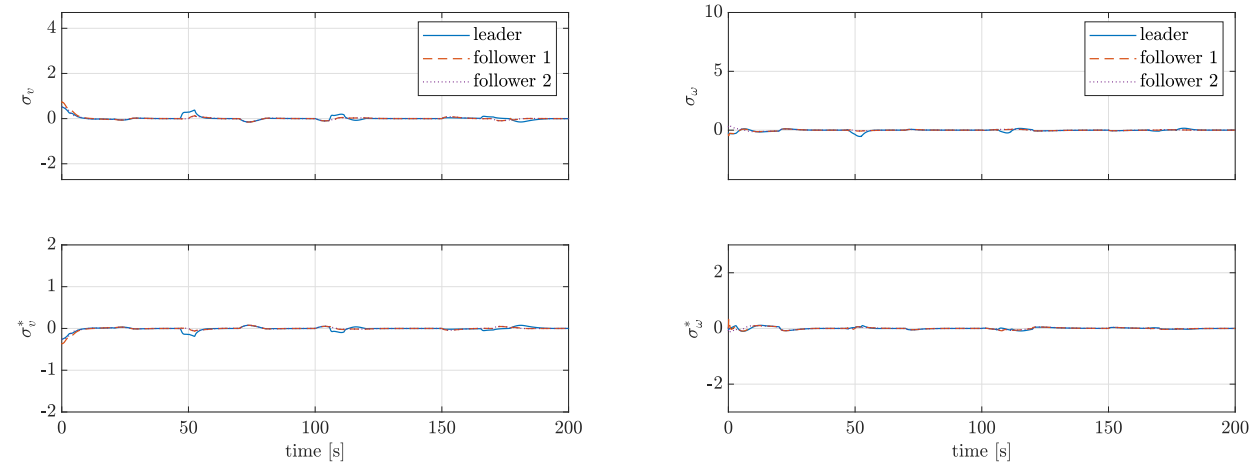

(a) Sliding surfaces σ_v and σ_v^*.

(b) Sliding surfaces σ_ω and σ_ω^*.

Figure 27: Sliding surfaces σ_n and σ_n^* (FCAFSMC).

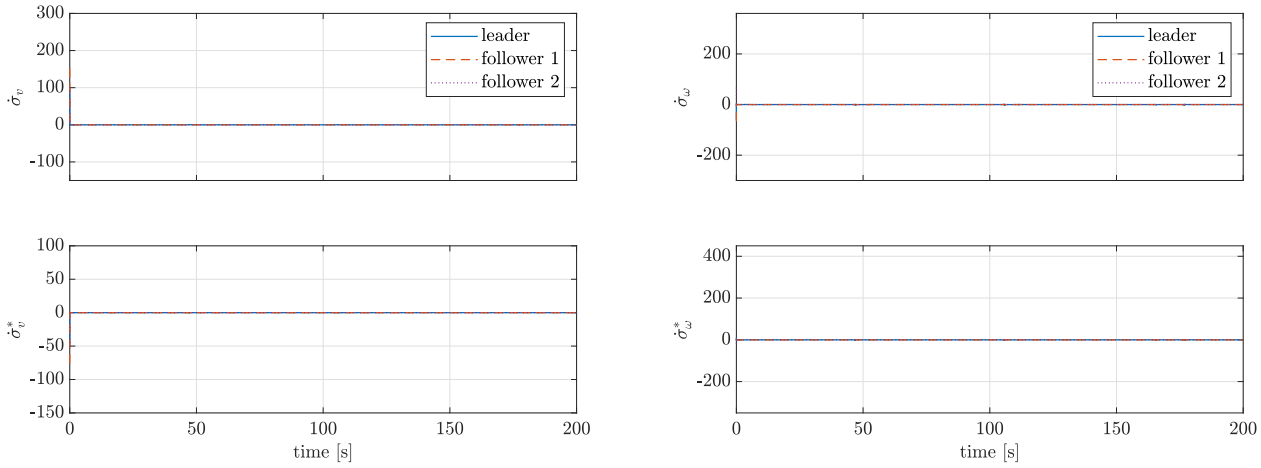

(a) Derivatives of sliding surfaces σ_v and σ_v^*.

(b) Derivatives of sliding surfaces σ_ω and σ_ω^*.

Figure 28: Derivatives of sliding surfaces σ_n and σ_n^* (FCAFSMC).

7.4 Experimental results for AIFQSMC

Results obtained of experimental simulations for the AIQFSMC were performed using the open-source simulator Gazebo connected to Matlab/Simulink via ROS interface. With the proposal of providing a smooth transition from simulation to real hardware, this tool is helpful in realistically testing and experiencing physical scenarios. In the experimental simulator, the obstacles are considered virtual, and the nonlinearities and uncertainties are just derived from the robotâs model in the Gazebo, with the model of the PowerBot DWMR being considered.

The RMSE values obtained are shown in the Table 13 and the graphical results are shown in Figs. 29a to 39b.

In summary, satisfactory performance in the trajectory tracking, formation, and OA was verified (Fig. 29a) with low levels of chattering (Fig. 29b). The proposed OA strategy worked adequately, as can be seen in Figs. 30a to 33b referring to the blending vectors generated for the OA, the reference posture (with the OA) compared with the original one (without OA), the variable avoidance radius for each obstacle and the relative distance between the DWMRs and the obstacles. The compensatory effect realized by the sliding mode control portion can be seen in Figs. 34a, 34b and 35a. The separation and bearing errors tend to be zero (Fig. 35b). The σ^*-trajectories considering time-varying boundary layers are shown in zoomed plots (Figs. 36a and 36b), observing that the sliding surfaces and their derivatives tended to zero (Figs. 37a and 37b). The signals generated in the AIS (Figs. 38a, 38b, 39a and 39b) provide the adaptation of the control actions.

Table 13: RMSE values – Experimental results (AIFQSMC).

	$RMSE(x_e)$	$RMSE(y_e)$	$RMSE(\theta_e)$
Leader	0.4604	0.5881	0.2205
Follower 1	0.1532	0.2428	0.1987
Follower 2	0.0999	0.1560	0.0349

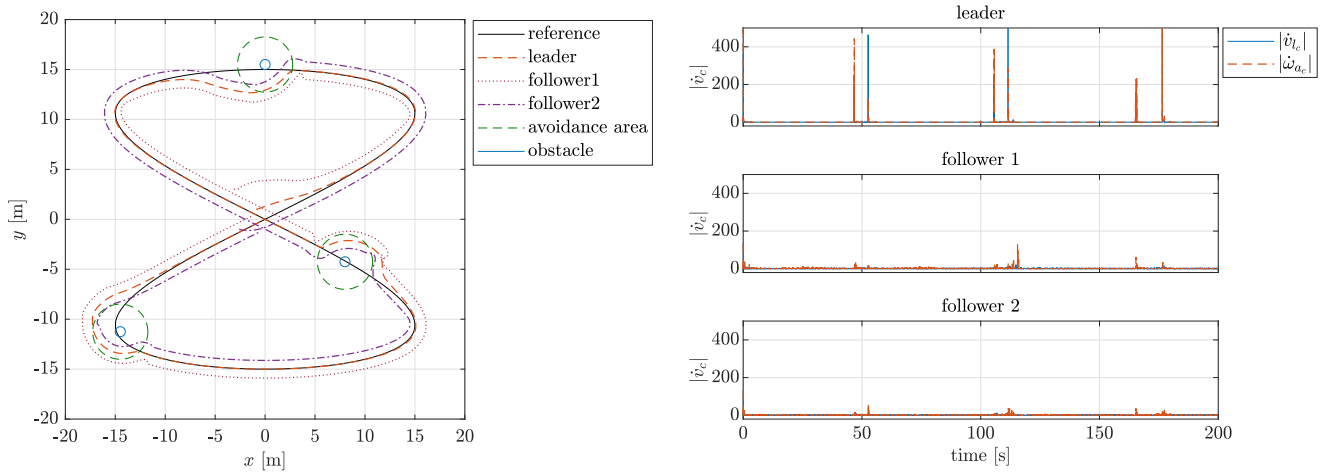

(a) Trajectory tracking, formation, OA.

(b) Chattering measure.

Figure 29: Trajectory tracking, formation, OA, and chattering measure (AIFQSMC) – Experimental.

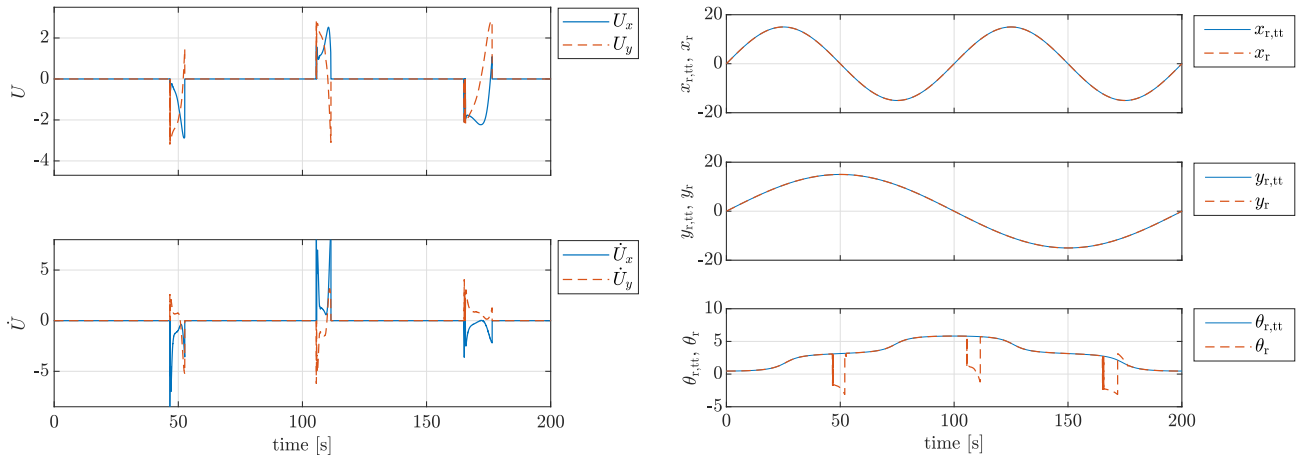

(a) OA blending vectors. (b) OA reference posture.

Figure 30: OA blending vectors, reference posture in original trajectory tracking and obstacle avoidance mode (AIFQSMC) – Experimental.

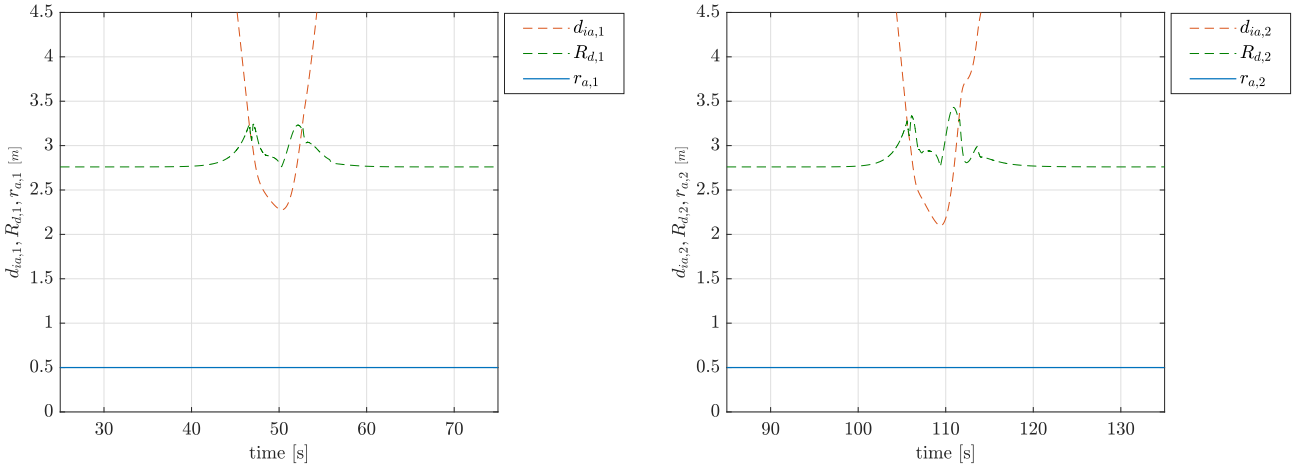

(a) $R_{d,1}$ (zoomed plot). (b) $R_{d,2}$ (zoomed plot).

Figure 31: Variable radii $R_{d,1}$ and $R_{d,2}$ (AIFQSMC) – Experimental.

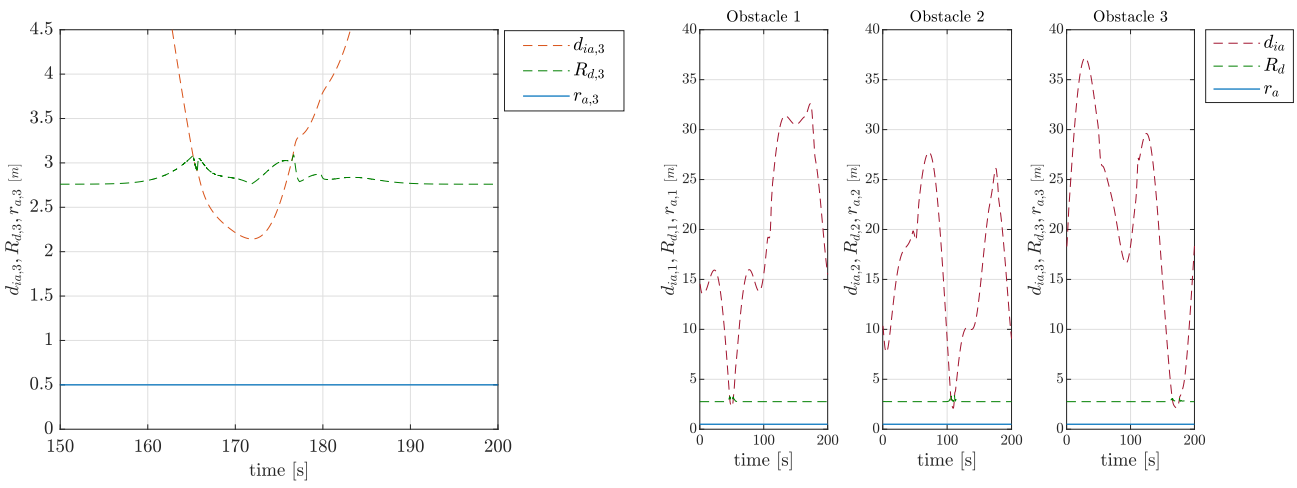

(a) $R_{d,3}$ (zoomed plot). (b) Relative distance between the leader DWMR and the obstacles.

Figure 32: Variable radius $R_{d,3}$ and relative distance between the leader DWMR and the obstacles (AIFQSMC) – Experimental.

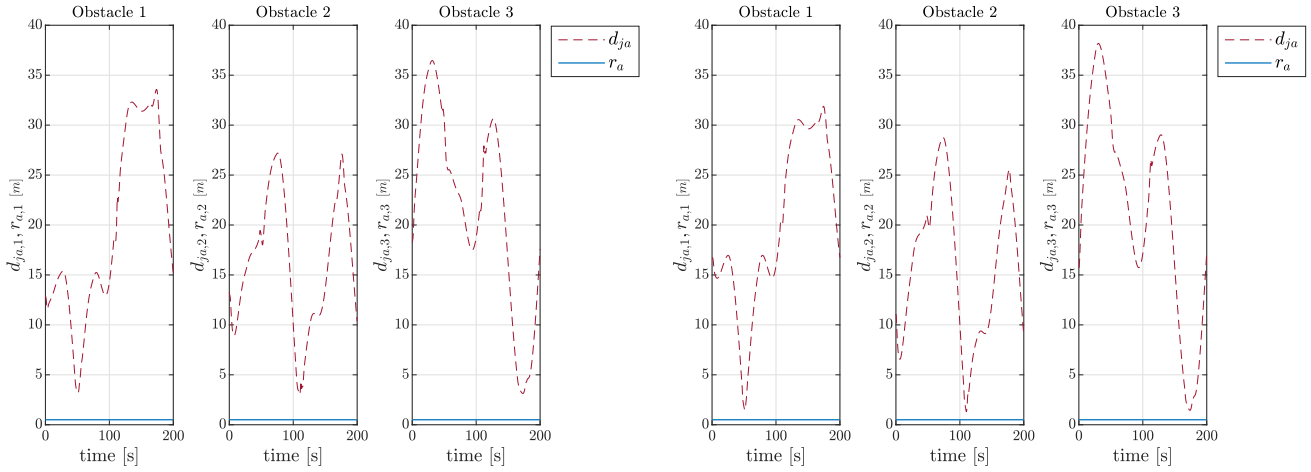

(a) Relative distance between the follower 1 DWMR and the obstacles.

(b) Relative distance between the follower 2 DWMR and the obstacles.

Figure 33: Relative distance between the followers DWMRs and the obstacles (AIFQSMC) – Experimental.

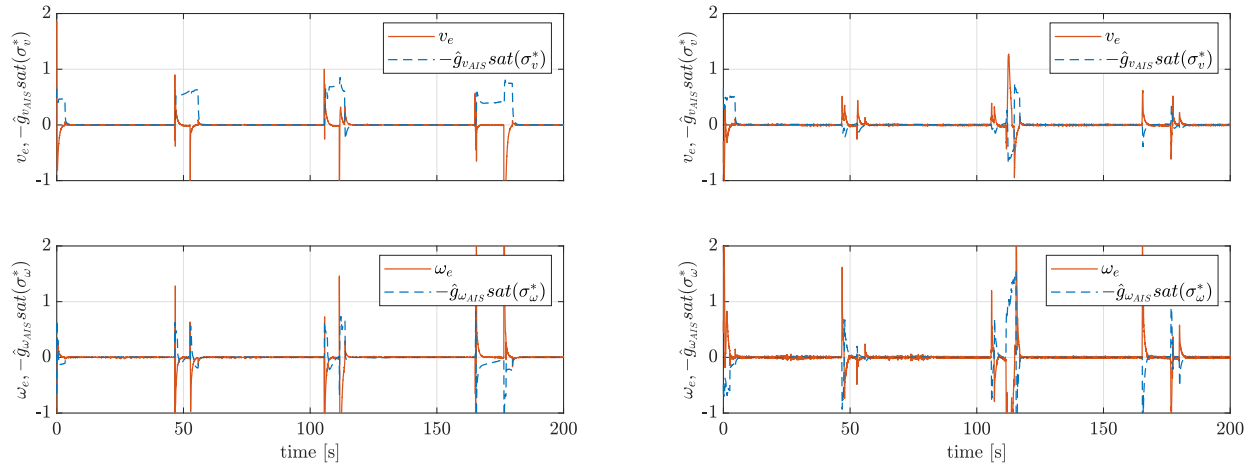

(a) Leader: Auxiliary velocity tracking errors and compensations.

(b) Follower 1: Auxiliary velocity tracking errors and compensations.

Figure 34: Auxiliary velocity tracking errors and compensations - Leader and Follower 1 (AIFQSMC) – Experimental.

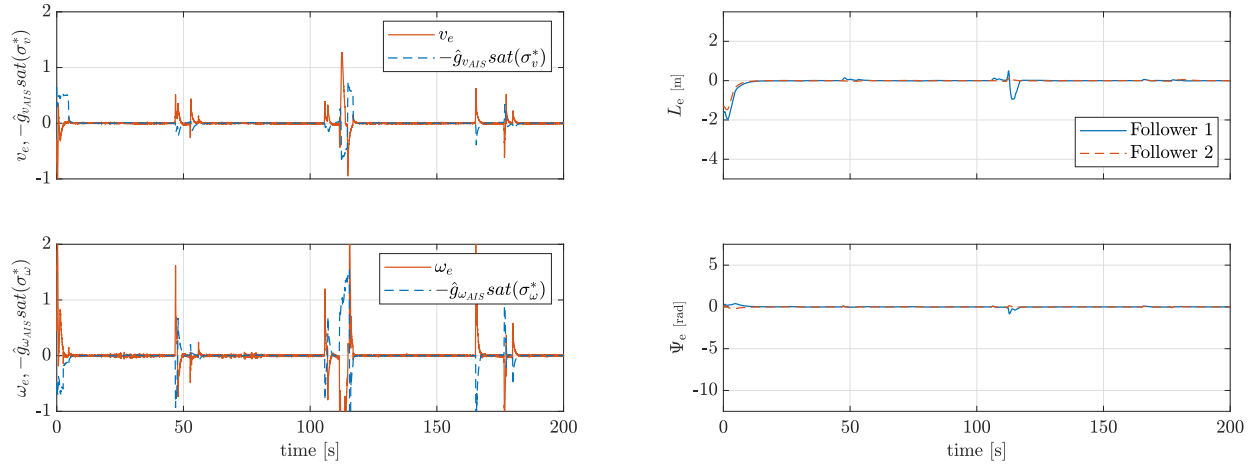

(a) Follower 2: Auxiliary velocity tracking errors and compensations.

(b) Separation and bearing errors.

Figure 35: Auxiliary velocity tracking errors and compensations - Follower 2 - and separation-bearing errors (AIFQSMC) – Experimental.

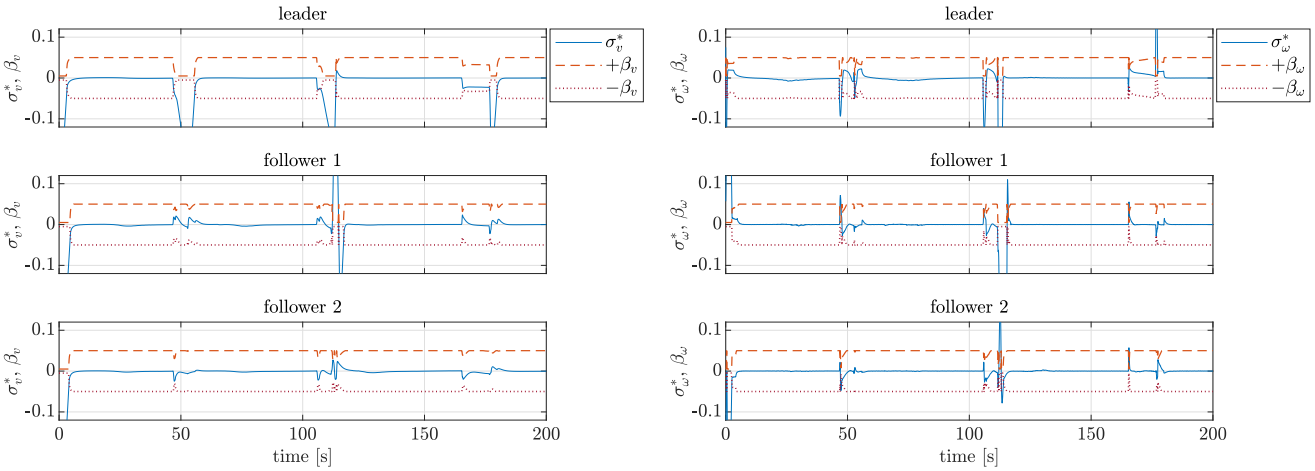

(a) σ_v^* and β_v. (b) σ_ω^* and β_ω.

Figure 36: σ_n^*-trajectories with time-varying boundary layer β_n (zoomed plot) (AIFQSMC) – Experimental.

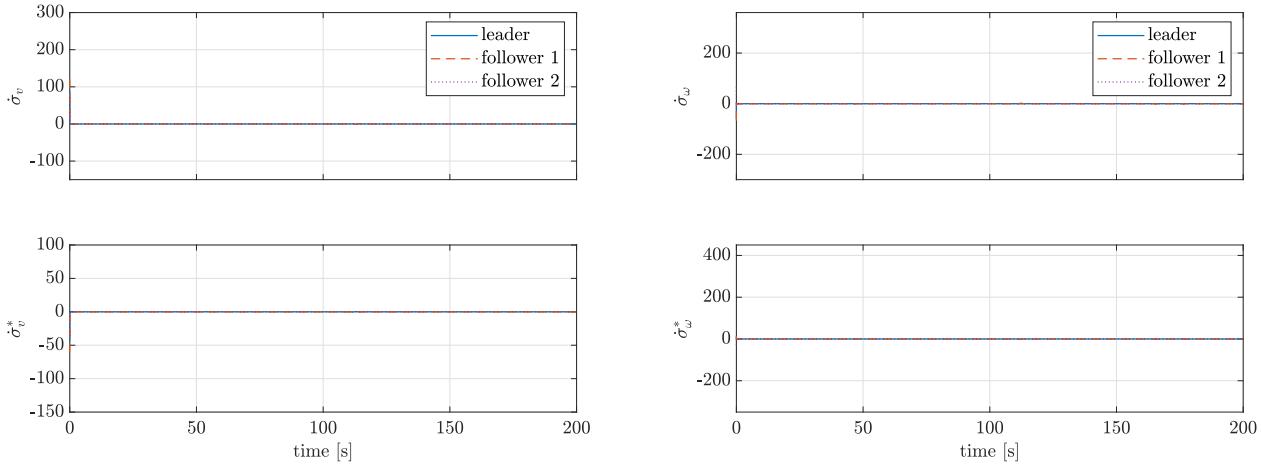

(a) $\dot{\sigma}_v$ and $\dot{\sigma}_v^*$. (b) $\dot{\sigma}_\omega$ and $\dot{\sigma}_\omega^*$.

Figure 37: Derivatives of sliding surfaces (AIFQSMC) – Experimental.

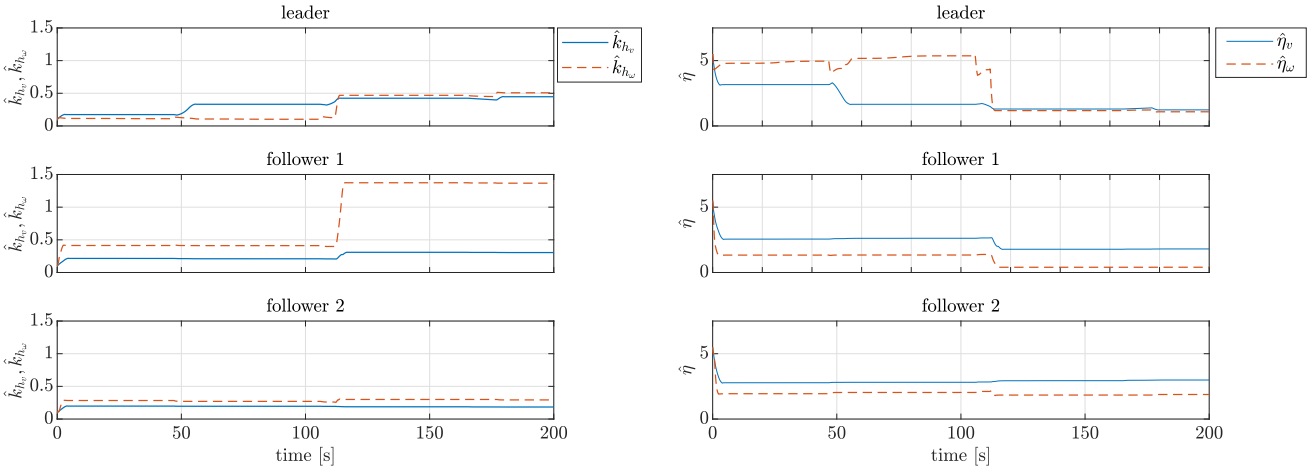

(a) Adaptive gains $\hat{k}_h$. (b) Time-varying parameter $\hat{\eta}$.

Figure 38: Adaptive gains $\hat{k}_h$ and $\hat{\eta}$ (AIFQSMC) – Experimental.

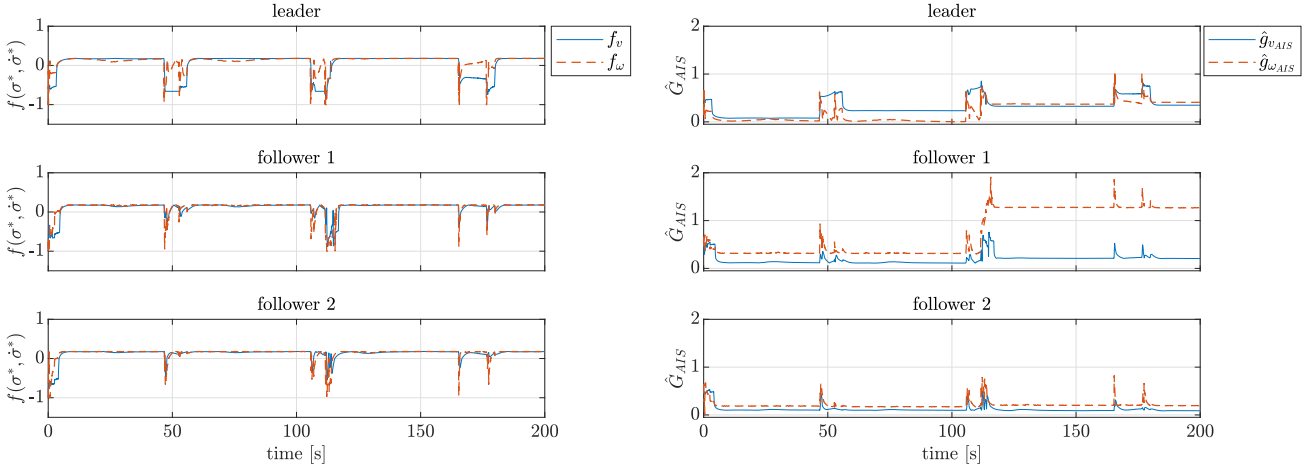

(a) AIS function $f(\sigma^*, \dot{\sigma}^*)$.

(b) AIS gain $\hat{G}_{AIS}$.

Figure 39: AIS function $f(\sigma^*, \dot{\sigma}^*)$ and gain $\hat{G}_{AIS}$ (AIFQSMC) – Experimental.

8 Conclusions

A leader-follower separation-bearing formation control was proposed for DWMRs under the incidence of uncertainties and disturbances in solving the trajectory tracking. The proposed kinematic controller AIFQSMC, inspired by an immune regulation mechanism, provided online adaptability for the SMC gains, without parameter drift, being able to smooth the control effort and to compensate uncertainties and disturbances without *a priori* knowledge of their upper bounds. The stability of the closed-loop control system was analyzed using the Lyapunov theory. Moreover, static obstacles distributed along the reference trajectory were considered to verify the adaptability of the AIFQSMC. The proposed obstacle avoidance strategy with the adjustable avoidance radius expansion made the leader DWMR reactively steer the obstacles.

Verifying the simulation results and comparing the different controllers, it was observed that the performance of the SMC was affected by its compensatory signals, which were limited by a constant gain. This problem was overcome by the AIFQSMC, whose gains were adaptively regulated thanks to the satisfactory functioning of the AIS and with an adjustment range improved by the proposed adaptation law. Chattering, another drawback of the SMC, was also significantly mitigated, counting on the fact that the fuzzy boundary layer also acted. Due to the performance equivalence with FCAFSMC, the AIFQSMC proves to be a convenient adaptive strategy alternative, attested by the results obtained from the experimental simulation.

Research can be extended to a comparison of AIFQSMC to other related approaches; generalization for other possible classes of mobile robots (i.e., unmanned aerial vehicles); and the treatment of inter-collision between DWMRs, dynamic obstacle avoidance problem, and the obstacle avoidance by the followers DWMRs, since they are still subject to a possible collision.

9 Acknowledgements

The authors would like to thank CAPES for its financial support.

REFERENCES

[1] B. Siciliano and O. Khatib. *Springer Handbook of Robotics*. Springer Publishing Company, Incorporated, second edition, 2016.

[2] V. Utkin, A. Poznyak, Y. Orlov and A. Polyakov. *Road Map for Sliding Mode Control Design*. Springer Cham, first edition, 2020.

[3] N. A. Martins and D. W. Bertol. *Wheeled Mobile Robot Control*. Springer International Publishing, 2022.

[4] H. Cen and B. K. Singh. "Nonholonomic wheeled mobile robot trajectory tracking control based on improved sliding mode variable structure". *Wireless Communications and Mobile Computing*, vol. 2021, pp. 1–9, 2021.

[5] B. Jiang, J. Li and S. Yang. "An improved sliding mode approach for trajectory following control of nonholonomic mobile AGV". *Scientific Reports*, vol. 12, no. 1, pp. 17763, 2022.

[6] A. D. Sabiha, M. A. Kamel, E. Said and W. M. Hussein. "ROS-based trajectory tracking control for autonomous tracked vehicle using optimized backstepping and sliding mode control". *Robotics and Autonomous Systems*, vol. 152, pp. 1–15, 2022.

[7] A. Y. Damani, Z. A. Benselama and R. Hedjar. "Formation control of nonholonomic wheeled mobile robots via fuzzy fractional-order integral sliding mode control". *International Journal of Dynamics and Control*, pp. 1–12, 2023.

[8] K. P. Kochumon, L. P. P. S and H. K. R. "Self-Tuning Backstepping and Sliding Mode Control for Robust Trajectory Tracking in Differential Drive Wheeled Mobile Robots". In *2023 International Conference on Power, Instrumentation, Control and Computing (PICC)*, pp. 1–6, April 2023.

[9] Y. Díaz, J. Dávila and M. Mera. "Leader-Follower Formation of Unicycle Mobile Robots Using Sliding Mode Control". *IEEE Control Systems Letters*, vol. 7, pp. 883–888, 2023.

[10] J. Minguez, F. Lamiraux and J.-P. Laumond. *Motion Planning and Obstacle Avoidance*, pp. 1177–1202. Springer International Publishing, Cham, 2016.

[11] L. Adouane. "Orbital Obstacle Avoidance Algorithm for Reliable and On-Line Mobile Robot Navigation". In *9th Conference on Autonomous Robot Systems and Competitions*, Castelo-Branco, Portugal, May 2009.

[12] F. L. Lewis and D. Vrabie. "Reinforcement learning and adaptive dynamic programming for feedback control". *IEEE Circuits and Systems Magazine*, vol. 9, no. 3, pp. 32–50, 2009.

[13] R. Bouchebbat. "Design and application of fuzzy immune PID control based on genetic optimization". In *International Workshop on Advanced Control IWAC*, pp. 10–14, 2014.

[14] L. Yu, Z. Cai, Z. Jiang and Q. Hu. "An Advanced Fuzzy Immune PID-type Tracking Controller of a Nonholonomic Mobile Robot". In *2007 IEEE International Conference on Automation and Logistics*, pp. 66–71, Aug 2007.

[15] X.-H. Liu, X.-H. Chen, X.-H. Zheng, S.-P. Li and Z.-B. Wang. "Development of a GA-fuzzy-immune PID controller with incomplete derivation for robot dexterous hand". *The Scientific World Journal*, vol. 2014, 2014.

[16] A. Dai, X. Zhou and X. Liu. "Design and simulation of a genetically optimized fuzzy immune PID controller for a novel grain dryer". *IEEE Access*, vol. 5, pp. 14981–14990, 2017.

[17] R. Bouchebbat and S. Gherbi. "Design and application of fuzzy immune PID adaptive control based on particle swarm optimization in thermal power plants". In *2017 6th International Conference on Systems and Control (ICSC)*, pp. 33–38. IEEE, 2017.

[18] P. Chu, Y. Yu, D. Dong, H. Lin and J. Yuan. "NSGA-II-based parameter tuning method and GM (1, 1)-based development of fuzzy immune PID controller for automatic train operation system". *Mathematical Problems in Engineering*, vol. 2020, 2020.

[19] H. Zhang, J. Hu and W. Bu. "Research on fuzzy immune self-adaptive PID algorithm based on new Smith predictor for networked control system". *Mathematical Problems in Engineering*, vol. 2015, 2015.

[20] G. Zhao, Y. Shen and Y. Wang. "Fuzzy PID Position Control Approach in Computer Numerical Control Machine Tool." *J. Comput.*, vol. 8, no. 3, pp. 622–629, 2013.

[21] X. Yu, F. Yang, Y. Huang and H. Nan. "Fuzzy immune sliding mode control based hydro turbine governor". In *Third International Conference on Natural Computation (ICNC 2007)*, volume 1, pp. 171–176, Aug 2007.

[22] X. Yu, F. Yang, Y. Huang and H. Nan. "Adaptive Fuzzy Immune Sliding Mode Control for a Class of Uncertain Nonlinear Systems". In *Fourth International Conference on Fuzzy Systems and Knowledge Discovery (FSKD 2007)*, volume 2, pp. 546–550, Aug 2007.

[23] X. Yu, J. Tian, Y. Huang and H. Nan. "Adaptive Double Immune Sliding Mode Control for a Class of Uncertain Nonlinear Systems". In *2008 IEEE International Conference on Fuzzy Systems (IEEE World Congress on Computational Intelligence)*, pp. 1199–1203, June 2008.

[24] W. B. Lin, H. K. Chiang and Y. L. Chung. "The Speed Control of Immune-Fuzzy Sliding Mode Controller for a Synchronous Reluctance Motor". In *Mechatronics and Applied Mechanics II*, volume 300 of *Applied Mechanics and Materials*, pp. 1490–1493. Trans Tech Publications Ltd, 5 2013.

[25] C. Sun, G. Gong and H. yong Yang. "Sliding Mode Control with Adaptive Fuzzy Immune Feedback Reaching Law". *International Journal of Control, Automation and Systems*, vol. 18, pp. 363–373, 2020.

[26] T. Dierks and S. Jagannathan. "Asymptotic Adaptive Neural Network Tracking Control of Nonholonomic Mobile Robot Formations". *Journal of Intelligent and Robotic Systems*, vol. 56, pp. 153–176, 2009.

[27] M. Begnini, D. W. Bertol and N. A. Martins. "A robust adaptive fuzzy variable structure tracking control for the wheeled mobile robot: Simulation and experimental results". *Control Engineering Practice*, vol. 64, pp. 27–43, 2017.

[28] E. S. Elyoussef, N. A. Martins, D. W. Bertol, E. R. D. Pieri and U. F. Moreno. "Simulation results and practical implementation of a PD-super-twisting second order sliding mode tracking control for a differential wheeled mobile robot". *International Journal of Computer Applications in Technology*, vol. 63, no. 3, pp. 213–227, 2020.

[29] T. Dierks and S. Jagannathan. "Control of Nonholonomic Mobile Robot Formations: Backstepping Kinematics into Dynamics". In *2007 IEEE International Conference on Control Applications*, pp. 94–99, Oct 2007.

[30] M. W. Spong, S. Hutchinson and M. Vidyasagar. *Robot modeling and control*. John Wiley & Sons, second edition, 2020.

[31] D. Dasgupta. "Advances in artificial immune systems". *IEEE Computational Intelligence Magazine*, vol. 1, no. 4, pp. 40–49, Nov 2006.

[32] Y. Peng, X. Luo and W. Wei. "A new control method based on artificial immune adaptive strategy". *Elektronika ir Elektrotechnika*, vol. 19, no. 4, pp. 3–8, 2013.

[33] C.-H. Wang and K.-C. Hor. "From Fuzzy Center Average Defuzzifier (CAD) to Fuzzy Lookup Table Controller (FLTC) with an Efficient Heaviside Search Algorithm (HSA)". *Neural Comput. Appl.*, vol. 31, no. 9, pp. 5135â5145, sep 2019.

[34] J.-J. E. Slotine and W. Li. *Applied nonlinear control*. Prentice hall, Englewood Cliffs, NJ, 1991.

[35] W. M. Bessa and R. S. S. Barrêto. "Adaptive fuzzy sliding mode control of uncertain nonlinear systems". *Sba: Controle & Automação Sociedade Brasileira de Automatica*, vol. 21, pp. 117–126, 2010.

[36] F. L. Lewis. "Nonlinear network structures for feedback control". *Asian Journal of Control*, vol. 1, no. 4, pp. 205–228, 1999.

[37] B. J. Emran and A. Yesildirek. "Robust nonlinear composite adaptive control of quadrotor". *International journal of digital information and wireless Communications*, vol. 4, no. 2, pp. 213–225, 2014.

[38] F. Plestan, Y. Shtessel, V. Brégeault and A. Poznyak. "Sliding mode control with gain adaptation – Application to an electropneumatic actuator". *Control Engineering Practice*, vol. 21, no. 5, pp. 679–688, 2013.

[39] V. I. Utkin and A. S. Poznyak. "Adaptive sliding mode control with application to super-twist algorithm: Equivalent control method". *Automatica*, vol. 49, no. 1, pp. 39–47, 2013.

[40] V. I. Utkin and A. S. Poznyak. "Adaptive sliding mode control". In *Advances in sliding mode control*, pp. 21–53. Springer, 2013.

[41] J. Zhu and K. Khayati. "Application of adaptive sliding mode control for nonlinear systems with unknown polynomial bounded uncertainties". *Transactions of the Institute of Measurement and Control*, vol. 40, no. 13, pp. 3721–3735, 2018.

[42] S. Roy, S. B. Roy, J. Lee and S. Baldi. "Overcoming the underestimation and overestimation problems in adaptive sliding mode control". *IEEE/ASME Transactions on Mechatronics*, vol. 24, no. 5, pp. 2031–2039, 2019.

[43] K. Erbatur and B. Çallı. "Fuzzy boundary layer tuning for sliding mode systems as applied to the control of a direct drive robot". *Soft Computing*, vol. 13, pp. 1099–1111, 2009.

[44] J. Guo, K. Li, J. Fan, Y. Luo and J. Wang. "Neural-Fuzzy-Based Adaptive Sliding Mode Automatic Steering Control of Vision-based Unmanned Electric Vehicles". *Chinese Journal of Mechanical Engineering*, vol. 34, no. 1, pp. 1–13, 2021.

[45] J. Zhu and K. Khayati. "Adaptive sliding mode control with smooth switching gain". In *2014 IEEE 27th Canadian Conference on Electrical and Computer Engineering (CCECE)*, pp. 1–6, May 2014.

[46] V. Brégeault, F. Plestan, Y. Shtessel and A. Poznyak. "Adaptive sliding mode control for an electropneumatic actuator". In *2010 11th International Workshop on Variable Structure Systems (VSS)*, pp. 260–265, June 2010.

[47] F. Plestan, Y. Shtessel, V. Bregeault and A. Poznyak. "New methodologies for adaptive sliding mode control". *International journal of control*, vol. 83, no. 9, pp. 1907–1919, 2010.

[48] J. A. Farrell and M. M. Polycarpou. *Adaptive approximation based control: unifying neural, fuzzy and traditional adaptive approximation approaches*. John Wiley & Sons, 2006.

[49] A. Ferrara and M. Rubagotti. "Second-order sliding-mode control of a mobile robot based on a harmonic potential field". *IET Control Theory & Applications*, vol. 2, no. 9, pp. 807–818, 2008.

[50] M. A. Kamel and Y. Zhang. "Decentralized leader-follower formation control with obstacle avoidance of multiple unicycle mobile robots". In *2015 IEEE 28th Canadian Conference on Electrical and Computer Engineering (CCECE)*, pp. 406–411, May 2015.

[51] J. Li, J. Sun and G. Chen. "A Multi-Switching Tracking Control Scheme for Autonomous Mobile Robot in Unknown Obstacle Environments". *Electronics*, vol. 9, no. 1, 2020.

[52] A. Benzerrouk, L. Adouane and P. Martinet. "Stable navigation in formation for a multi-robot system based on a constrained virtual structure". *Robotics and Autonomous Systems*, vol. 62, no. 12, pp. 1806–1815, 2014.

[53] A. Ferrara and M. Rubagotti. "Sliding mode control of a mobile robot for dynamic obstacle avoidance based on a time-varying harmonic potential field". In *ICRA 2007 Workshop: Planning, Perception and Navigation for Intelligent Vehicles*, volume 160. Citeseer, 2007.

[54] M. Mancini, N. Bloise, E. Capello and E. Punta. "Sliding Mode Control Techniques and Artificial Potential Field for Dynamic Collision Avoidance in Rendezvous Maneuvers". *IEEE Control Systems Letters*, vol. 4, no. 2, pp. 313–318, April 2020.

[55] M. Gu and Y. Huang. "Dynamic Obstacle Avoidance of Mobile Robot Based on Adaptive Velocity Obstacle". In *2021 36th Youth Academic Annual Conference of Chinese Association of Automation (YAC)*, pp. 776–781, May 2021.

[56] A. Ferrara and M. Rubagotti. "A dynamic obstacle avoidance strategy for a mobile robot based on sliding mode control". In *2009 IEEE Control Applications, (CCA) & Intelligent Control, (ISIC)*, pp. 1535–1540, July 2009.

[57] A. Nikranjbar, M. Haidari and A. A. Atai. "Adaptive sliding mode tracking control of mobile robot in dynamic environment using artificial potential fields". *Journal of Computer & Robotics*, vol. 11, no. 1, pp. 1–14, 2018.

[58] A. Rosales, G. Scaglia, V. Mut and F. di Sciascio. "Trajectory tracking of mobile robots in dynamic environments – a linear algebra approach". *Robotica*, vol. 27, no. 7, pp. 981â997, 2009.

[59] J. Vilca, L. Adouane and Y. Mezouar. "Adaptive Leader-Follower Formation in Cluttered Environment Using Dynamic Target Reconfiguration". In *Distributed Autonomous Robotic Systems*, edited by N.-Y. Chong and Y.-J. Cho, pp. 237–254, Tokyo, 2016. Springer Japan.

[60] F. P. Freire, N. A. Martins and F. Splendor. "A simple optimization method for tuning the gains of PID controllers for the autopilot of cessna 182 aircraft using model-in-the-loop platform". *Journal of Control, Automation and Electrical Systems*, vol. 29, pp. 441–450, 2018.

[61] J. Zhang, D. Wei, R. Gao and Z. Xia. "A trajectory tracking and obstacle avoidance approach for nonholonomic mobile robots based on model predictive control". In *2020 IEEE 16th International Conference on Control & Automation (ICCA)*, pp. 1038–1043, Oct 2020.